Dissertationes Forestales 277

Utilizing multispectral lidar in the detection of declined trees

Samuli Junttila

Department of Forest Sciences
Faculty of Agriculture and Forestry
University of Helsinki

Academic dissertation

To be presented with the permission of the Faculty of Agriculture and Forestry, University of Helsinki, for public criticism in the 235 auditorium of the Korona-building (Viikinkaari 7) on June 7th, 2019, at 12 o'clock.

Title of dissertation: Utilizing multispectral lidar in the detection of declined trees

Author: Samuli Junttila

Dissertation Forestales 277

https://doi.org/10.14214/df.277

Thesis Supervisors:
Professor Markus Holopainen
Department of Forest Sciences, University of Helsinki, Finland

Associate professor Mikko Vastaranta
Department of Forest Sciences, University of Eastern Finland, Joensuu, Finland

Pre-examiners:
Professor Hans Verbeeck
Department of Environment, Ghent University, Belgium

Docent Mikko Peltoniemi
Natural Resources Institute Finland, Helsinki, Finland

Opponent:
Docent Tuomo Kauranne
Arbonaut Ltd., Joensuu, Finland

ISSN 1795-7389 (online)
ISBN 978-951-651-644-1 (pdf)

ISSN 2323-9220 (print)
ISBN 978-951-651-645-8 (paperback)

Printers:
Unigrafia, Helsinki 2019

Cover:
Samuli Junttila

Publishers:
Finnish Society of Forest Science
Faculty of Agriculture and Forestry of the University of Helsinki
School of Forest Sciences of the University of Eastern Finland

Editorial office:
Finnish Society of Forest Science
Viikinkaari 6, FI-00790 Helsinki, Finland
http://www.dissertationesforestales.fi

Junttila S. (2019). Utilizing multispectral lidar in the detection of declined trees. Dissertationes Forestales 277. 58 p. https://doi.org/10.14214/df.277

ABSTRACT

The World's forests are facing novel stress due to climate change. Pest insects and pathogens are shifting towards new latitudes and heat stress is resulting in increased tree mortality and more frequent forest fires globally. Uncertainty in estimating the magnitude of climate change induced forest and tree decline requires new methods for unbiased estimation of tree decline. The development of remote sensing methods to detect early tree decline has been a major challenge due to the subtle nature of the early changes caused by different stressors. Multispectral lidar technology has the potential of detecting early tree decline by providing accurate three-dimensional and spectral information of tree structure simultaneously.

The main objective of this thesis was to investigate the capabilities of multispectral terrestrial lidar in the detection and assessment of tree decline caused by different stressors. This was done by investigating the estimation of a remotely detectable indicator of tree decline, leaf water content (LWC). Specifically, new methods for measuring LWC using multispectral lidar intensity were developed from the leaf to the canopy scale in various environments and the relationship between LWC and tree decline induced by various stressors was investigated. Furthermore, the developed methods were tested in a forest environment to assess the applicability of multispectral lidar in the detection of bark beetle infestation in the field.

Studies I-III focused on investigating the relationship between LWC and lidar intensity at multiple wavelengths. First, a hyperspectral lidar instrument was used to detect significant changes between fresh and drought-treated Scots pine (*Pinus sylvestris* L.) and Norway spruce (*Picea abies* L.) trees (study I). Then, a leaf-scale study (II) with Scots pine, Norway spruce, Small-leaved lime (*Tilia cordata* L.), Norway maple (*Acer platanoides* L.) and Silver birch (*Betula pendula* L.) was conducted and a strong relationship (R^2=0.93) between a normalized difference index (NDI) calculated from 1550 nm and 690 nm wavelengths and LWC was found. This was followed by a study (III) where LWC estimation and pathogen- and drought-induced variation in LWC was studied with Norway spruce seedlings. Blue-stain fungi (*Endoconidiophora polonica*) inoculated seedlings expressed a rapid decrease in LWC while drought-treated seedlings showed more stable LWC until a very severe drought. LWC of the seedlings was predicted with an R^2 of 0.89 using an NDI with 1550 nm and 905 nm wavelengths.

In study IV, the developed method and the relationship between LWC and tree decline was investigated in the field with European spruce bark beetle (*Ips typographus* L.) infested trees. It was found that of the LWC metrics studied, gravimetric water content showed significant differences in the early stages of infestation and was more sensitive to bark beetle induced tree decline than equivalent water thickness (i.e. amount of water per leaf area). Linear discriminant models that were developed between infestation severity and lidar intensity metrics from 1550 nm and 905 nm wavelengths showed that green attack stage of the infestation could classified with an overall accuracy of 90%.

This dissertation contributes both to the development of an objective and automatable method for detecting and measuring tree decline in the field, and to the understanding of the relationship between LWC and tree decline with implications to remote sensing. The dissertation will be published and popularized as a music video here: http://bit.ly/idanproffa.

Keywords: remote sensing, terrestrial laser scanning, LiDAR, tree health, leaf water content, forest decline

ACKNOWLEDGEMENTS

The first steps towards this dissertation were taken by accident in 2014 as I was doing my master's thesis project. My supervisor Markus Holopainen mentioned that an extra month of funding was available if I was willing to write a scientific article about my master's thesis. Sure, I said, whilst thinking that this is easy money, and there I was on the edge of entering the realm of science not knowing what was going to be ahead. Eventually (as you can imagine), a single month was not nearly enough to get the scientific article through the wheels of the scientific publishing machinery, but luckily Markus invited me to attend one of the meetings of the Center of Excellence. I was thinking that what the hell a not even M.Sc. newbie like me was doing among the well-established professors and scientists in the workshop, trying to act like I knew something about the business. But thinking afterwards, it was clearly a strategic move from Markus. I had published a photograph in the prestigious Nature journal during my summer work in Hyytiälä forest field station, which impressed some of the other professors. It was not long before Hannu Hyyppä from the department of built environment in Aalto university came to talk to me saying out of the blue: "I have money, let's write a work contract for you." It was pretty much a no-brainer to think what to answer. These events gave a good kick-start for my PhD project and I would like to thank Markus and Hannu for believing in me from the very beginning.

I have been very lucky to be able to work with a very talented set of colleagues. Mikko Vastaranta was there to help me out with planning and implementing the experiments since my master's thesis project, working as my supervisor in the dissertation with Markus. There was a clear work division between the two from the start: Markus arranged the resources and funding and Mikko helped with the scientific content and gave feedback. A very good team I must say! Many thanks to Juha Hyyppä, Harri Kaartinen and Antero Kukko from FGI, whom have helped me with getting and operating the instruments that were needed for conducting the experiments in this dissertation. This dissertation would not had been possible without your help. Thanks also to Xinlian Liang and Sanna Kaasalainen, whom helped with the first studies and provided insight to the mathematics. I would also like to thank Eija Honkavaara, who provided funding and gave me the possibility to travel to Brazil to do field work. Thanks to Teemu Hakala and Olli Nevalainen for providing some important measurements.

The topic of this dissertation is highly cross-disciplinary, which has opened a range of cooperation possibilities outside the field of remote sensing. Riikka Linnakoski was in a crucial position in enabling the third study and I am very happy that she took me along to the experiment in Läyliäinen. We had a really nice time and thanks to Junko Sugano for helping with the measurements. Thanks to Päivi Lyytikäinen-Saarenmaa, the dissertation got an excellent nice final study that was conducted in Ruokolahti, a fine example of cross-disciplinary science as well. Thanks to Pentti Henttonen, Jaana Turunen and Minna Blomqvist for assisting with the field measurements.

A special thanks goes also to all the members of our research group! Topi Tanhuanpää was sitting next to me for a major part of the work conducted and gave important peer support. Thanks to Ville Luoma, Ninni Saarinen, Ville Kankare, Jiri Pyörälä, Tuomas Yrttimaa, Einari Heinaro, Mohammad Imangholiloo and Joanne White for all the lunches, travels, cooperation and discussions we have had. I would also like to thank all the colleagues and members of staff at the department of forest sciences at the University of Helsinki for all the support and assistance. A special thanks goes to Pasi Puttonen who has been supporting my work in the background all these years.

Finally, but definitely not last, I would like to thank my family for supporting and enduring during these years of PhD work. It has not always been easy to live with me as I have had so many projects in addition to the PhD during these last years. Thanks to Rosa Virmajoki, to my precious wife, for enduring all the travels and extra work! This would not had been possible without your support. Thanks also to my kids, Asa and Oula, for being such good boys and giving me so much happiness and love to my life.

I would have never got into this point without the support from my parents, my father Jouko Junttila and my mother Anna-Liisa Salminen. I have been so lucky to be raised in a safe and supporting environment that has given me the resources to aim where ever I have wanted at with confidence. My mom, a recent professor, has set the example for me in science and my dad has shown me how to build things and enjoy life. They have also been of great assistance during my PhD project. My mom enabled me to work while I was home with my youngest by taking care of him and my dad helped with renovating our new apartment, enabling me to focus on my PhD. Thanks to my little sister Sallamaari for being such a lovely sister and helping with everything when in need. Thanks to Päivi and to my step bros Mikko, Juuso and Samuli for being in my life. Many thanks also to the Virmajoki family, which have helped always when in need of assistance.

Many thanks go also to my colleagues at the mansion of Rastila, where I have been working for the last year of my dissertation. It has been a superb working environment and Henkka, Mete, Mihkel, Jere, Teemu, Simo and Jussi have been of great company and have also helped in getting the results of the dissertation to the people in the form of a music video. Thanks to Sami Tammela and Linda Ilves for helping me to create a great song about the dissertation. Thanks to Kaisa, Emmi and Ronja for all the superb moves for the music video. Thanks to Olli Ernvall for helping me with the planning of the communication of the dissertation. A special thanks goes to all my friends who give me love and friendship and help me to relax during my free time.

This dissertation would not have been possible without financial assistance from various sources: Center of Excellence in Laser Scanning Research funded by Academy of Finland, Niemi-foundation, the Finnish Society of Forest Science, Finnish cultural foundation, Otto A. Malm foundation, University of Helsinki, Academy of Finland project “Unmanned Airborne Vehicle–based 4D Remote Sensing for Mapping Rain Forest Biodiversity and Its Change in Brazil”. Thank you to them for making this PhD project and all my travels to conferences possible.

Helsinki, May 2019

Samuli Junttila

LIST OF ORIGINAL ARTICLES

This thesis is based on the following research articles, which are referred to in the text by their Roman numerals. Articles I–III are reprinted with the permission of the publishers. Article IV is an author version of a manuscript sent for review.

I Junttila, S., Kaasalainen, S., Vastaranta, M., Hakala, T., Nevalainen, O. ja Holopainen, M. (2015). Investigating Bi-Temporal Hyperspectral LiDAR Measurements from Declined Trees—Experiences from Laboratory Test. Remote Sensing 7 (10): 13878-13894.
http://dx.doi.org/10.3390/rs71013863

II Junttila, S., Vastaranta, M., Liang, X., Kaartinen, H., Kukko, A., Kaasalainen, S., Holopainen, M., Hyyppä, H. ja Hyyppä J. (2017). Measuring leaf water content with dual-wavelength intensity data from terrestrial laser scanners. Remote Sensing 9 (8).
http://dx.doi.org/10.3390/rs9010008

III Junttila, S., Sugano, J., Vastaranta, M., Linnakoski, R., Kaartinen, H., Kukko, A., Holopainen, M., Hyyppä, H. ja Hyyppä J. (2018). Can leaf water content be estimated using multispectral terrestrial laser scanning? A case study with Norway spruce seedlings. Frontiers in Plant Science 9:299.
http://dx.doi.org/10.3389/fpls.2018.00299

IV Junttila, S., Vastaranta, M., Holopainen, M., Lyytikäinen-Saarenmaa, P., Kaartinen, H., Hyyppä, H. ja Hyyppä J. (2019). The potential of dual-wavelength terrestrial lidar in early detection of *Ips typographus* (L.) infestation – leaf water content as a proxy. Manuscript. Submitted to Remote Sensing of Environment.

AUTHOR CONTRIBUTION

(I) Junttila wrote the first version of the manuscript and analyzed the lidar data. Kaasalainen designed the test and contributed to improving the manuscript. Vastaranta contributed to improving the manuscript and organizing the cooperation between FGI and University of Helsinki. Hakala and Nevalainen conducted the measurements and processed the data. Holopainen commented the manuscript and provided required resources.

(II) Junttila designed the experiment, conducted the statistical analysis, and wrote the manuscript. Vastaranta assisted in planning the experiment design, contributed to analyzing the data, and commented on the manuscript. Liang contributed to designing of the experiment and commented the manuscript. Kaartinen and Kukko assisted with setting up the measurement setup and provided technical advice. Kaasalainen contributed to improving the intensity correction methods. Holopainen, Hannu Hyyppä, and Juha Hyyppä arranged all the required resources for conducting the experiment, supervised the experiment, and participated in the writing of the manuscript.

(III) Junttila designed the experiment, conducted lidar data processing and statistical analysis of the data, and wrote the manuscript. Sugano assisted in laboratory analysis and writing of the manuscript. Vastaranta helped in designing the experiment, analyzing the data, and drafting the manuscript. Linnakoski contributed to designing the experiment, collecting the data, and commented on the manuscript. Kaartinen helped to design the experiment, gave technical advice, and commented on the manuscript. Kukko assisted with the measurement setup and provided technical support. Holopainen, Hannu Hyyppä, and Juha Hyyppä arranged all the required resources, supervised the experiment, and participated in the writing of the manuscript.

(IV) Junttila planned the experiment, conducted data processing and statistical analyses and wrote the first draft of the manuscript. Holopainen contributed to improving the manuscript and provided required resources. Vastaranta assisted in planning the experiment and improving the manuscript. Lyytikäinen-Saarenmaa helped in planning the experiment, provided resources for the data collection and commented on the manuscript. Kaartinen commented on the manuscript and provided technical support. Juha Hyyppä commented on the manuscript. Hannu Hyyppä provided required resources and commented on the manuscript.

TABLE OF CONTENTS

ABBREVIATIONS

3D	Three-dimensional
EWT	Equivalent water thickness
FMC	Fuel moisture content
GWC	Gravimetric water content
HSL	Hyperspectral lidar
LMA	Leaf mass per area
LRI	Laser ratio index
LWC	Leaf water content
NDI	Normalized difference index
NDVI	Normalized difference vegetation index
NLDI	Normalized laser difference index
NIR	Near infrared (λ = 700-1100 nm)
RGB	Red green blue
RMSE	Root mean square error
RS	Remote sensing
SR	Simple ratio
SWIR	Shortwave infrared (λ = 1100-3000 nm)
TLS	Terrestrial laser scanning, terrestrial lidar

1. INTRODUCTION

1.1 What is tree decline?

Forests are one of the most important natural resources and provider of ecosystem services on our planet. Forests and trees provide food, medicine and fuel for more than a billion people, protect soils and water, and clean the air (FAO 2018). Forests are a home for over 75% of the terrestrial species on this planet and forest growth sequesters about 30% of annual anthropogenic emissions, equivalent of roughly 2 billion tonnes of carbon dioxide (Houghton and Nassikas 2018). Forests play a vital role in stopping and mitigating the effects of climate change, but their ability to mitigate climate change and sequester carbon largely depends on the health condition of forests (Allen et al. 2015; Ellison et al. 2017).

Tree decline is defined as a prolonged malfunction of tree functions, such as defoliation, lowered photosynthetic activity or discoloration of leaves, within this dissertation (Jurskis 2005). Every functionality of a tree exhibits natural variability that occurs within different time scales (Van Gelder et al. 2006). Photosynthetic activity varies daily according to the flux of incoming photosynthetically active radiation a tree receives, i.e., less photosynthesis occurs on a cloudy day and more on a clear day (Hesketh 1963). The amount of foliage can vary yearly according to environmental conditions, such as precipitation or temperature (Watson 1958). The magnitude of the variation is not necessarily very significant, but some variation is always occurring, i.e. no function is in a completely steady state through the life of a tree (Reich et al. 1998). The magnitude of the variation varies with age, site conditions and climatic conditions (Dittmar et al. 2003). A declined tree is not functioning typically to its environmental conditions and is out of the normal variation of tree functionality (Figure 1). The decline can be temporary or permanent depending on the consequences of the decline. A temporary decline leads to recovery of tree functions at some point of time and a permanent decline results eventually in tree death that may be facilitated by pathogens, pest insects or abiotic environmental conditions, such as drought and fire.

The underlying reasons of tree decline can be complex. In the past decades tree decline in Europe and North America has been widely attributed to pollution and toxic chemicals in the atmosphere, soils and waters (Schulze 1989; Kandler 1992; Kreutzer 1993). Ozone, as an atmospheric oxidant, has been identified as a source of tree decline in eastern North America (Chevone and Linzon 1988). Since the 1990s, the amount of pollutants in the ecosystems has decreased in developed parts of the world due to more sophisticated catalysator systems in cars and industrial plants, a trend driven by governmental regulation (Bosteels and Searles 2002).

Currently, the global trends in tree decline and tree dieback can be largely attributed to climate change that is causing novel tree decline (Auclair 1993; Williams et al. 2013; Allen et al. 2015). Climate change is driving a decline in forest productivity and tree survival that has been documented at many sites globally (Williams et al. 2013). The causes of decline can be attributed to a variety of novel biotic and abiotic stressors that are related to changes in temperature and precipitation. Higher temperatures increase forest drought-stress and can lead to widespread tree mortality, but the threshold which leads to mortality is not well known (Choat et al. 2012; Williams et al. 2013; Allen et al. 2015). Drought-stress can increase the intensity of pest insect infestations and pathogen infections, increasing the damage caused by defoliators and secondary agents living on woody organs (Figure 2) (Jactel et al. 2012). Shifts in pest insect range towards northern latitudes are likely to occur with warming climate, potentially causing widespread damage to forests not accustomed to the invasive species (Netherer and Schopf 2010). The projection of the on-going climate change and the

evaluation of the effects of stress intensification is a challenging task and requires systems to assess and monitor the health of global forests with an emphasis on the early-detection of forest decline (Trumbore et al. 2015).

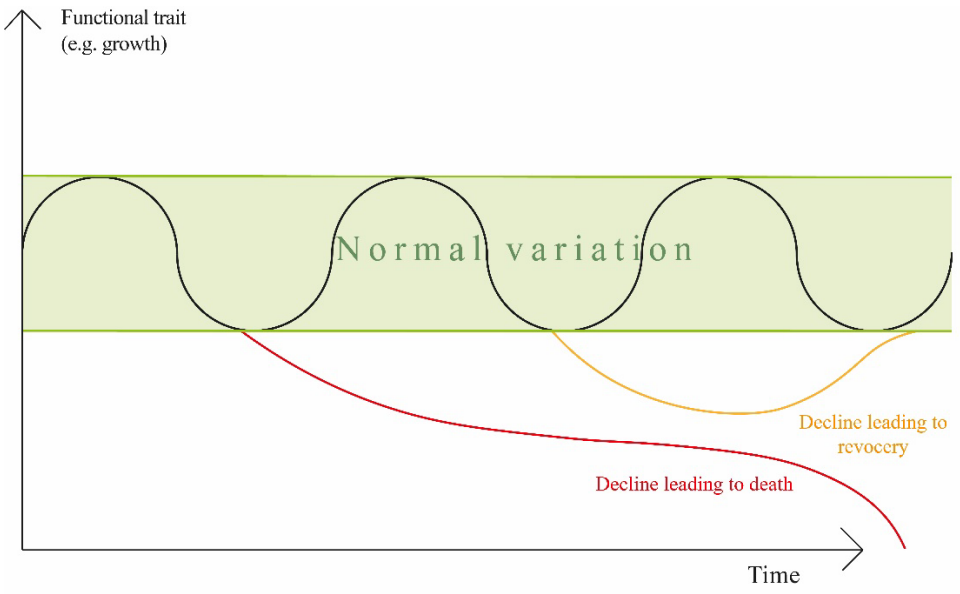

Figure 1. Variation of tree functions with time.

Figure 2. *Ips typographus* induced bark damage on Norway spruce stem.

Economically the most important coniferous tree species in Europe is Norway spruce (*Picea abies* (L.) Karst.) contributing more than 60% of the total economic value of tree species in Europe (Schlyter et al. 2006; Hanewinkel et al. 2013). The species is also of national economic importance, as forestry is a major economic activity in northern and north-eastern parts of Europe. The effects of climate change on Norway spruce have been modelled using climate scenarios (Schlyter et al. 2006; Hanewinkel et al. 2013) concluding that the frequency and duration of extreme climate events will increase, adding to the susceptibility of Norway spruce to pests and pathogens (Schlyter et al. 2006). Decreased forest vitality can result in greater amounts of windthrown areas despite the small increase in wind speeds and frequency of storms, resulting in exponential growth of feed for the European spruce bark beetle (*Ips typographus* L.) (Schlyter et al. 2006). The combination of higher mean temperatures and increased feed amount can result in additional *I. typographus* generations and mass outbreaks that can pose a threat to the health condition of forests (Wermelinger 2004). Forest decline and changing climate have been estimated to lead to a significant decrease in areas that are suitable for the cultivation of Norway spruce in Europe, resulting in an economic loss of more than 190 billion euros in forest-land value by the year 2100 (Hanewinkel et al. 2013).

1.2 Remote sensing of tree decline

Forest health assessments have been traditionally based on visual estimation from the air or ground, which is expensive and prone to error and bias due to the subjective nature of the estimation. Visual mapping of forest damage that can cover larger areas are done from helicopters or airplanes and are based on the color and amount of foliage of trees, which does not allow for the detection of subtle changes or early signals that precede tree decline. Another long-used method to assess tree vigor, growth and probability of tree mortality is the measurement of stem wood production by measuring annual ring width or basal area increment (Fritts 1976; Waring 1983). There has been some evidence that the reduction in stem wood production due to stress can be linked to even greater reduction in defensive compounds making the tree susceptible to attack by a variety of insects and pathogens (Waring and Pitman 1985; LeBlanc et al. 1992). Obviously, measuring tree rings or growth is a highly intensive and time-consuming process, thus, new methods are needed for accurate and subjective estimation of forest health for detecting declined trees.

Remote sensing (RS) methods that have been used to detect and monitor forest decline or forest health can be divided by scale: from leaf-level close-range measurements to airborne sensing for stand-level or tree-level measurements to satellite-based methods for large-scale monitoring (Wang et al. 2010; Lausch et al. 2017). The scale and intensity of forest decline varies across continents along with the intensity of forest management, and thus, the requirement for spatial resolution depends on the type and the scale of the decline event. Generally, the larger the extent of the decline event, the coarser resolution RS data can be used for detecting forest decline. Earth observation missions, such as the Landsat mission or Copernicus programme, enable the collection of long time-series satellite imagery which assists in the detection of forest decline (Anderson et al. 2010; Kennedy et al. 2010; Vogelmann et al. 2012).

Several studies have shown that existing RS methods can detect significant forest and tree decline, such as tree mortality, severe defoliation or discoloration, with relatively high accuracy using satellite observations (Wulder et al. 2006). Most of the studies conducted so far, however, lack in the detection accuracy of subtle or small-scale forest decline events and only few methods have shown potential in the detection of early forest decline (Immitzer and

Atzberger 2014; Abdullah et al. 2018). The early-detection of forest decline is crucial for timely forest management operations, and for maintaining the ecosystem services forests provide. High-resolution RS methods have the potential to provide an objective estimate of forest condition that is not biased by visual interpretation.

1.3 Terrestrial lidar systems and data acquisition

Terrestrial lidar (i.e. terrestrial laser scanning (TLS)) is a technique for measuring three-dimensional coordinates of targets or surfaces using laser light from a terrestrial position. TLS instruments that are used in vegetation mapping utilize two different methods for range measurement: round trip time of a light pulse and phase comparison of a continuous wave (Lemmens 2011). The pulse-based systems send nano-second pulses of laser light that is reflected from the target object. The scanner detects the reflected laser light and the distance between the scanner and the object is calculated based on the time measurement between the sent and the received pulse. Phase-based systems send a continuous laser light wave that is modulated with a harmonic signal. The scanner sensor measures the phase difference between the emitted and the received signal and calculates distance to the object. Both systems generally utilize a rotating mirror for sending and receiving the laser light in a regular grid pattern.

TLS can utilize different wavelengths in the laser source. Technical aspects and eye-safety limit the amount wavelengths that can be used in commercial scanners due to high amount of energy carried by shorter wavelengths. Popular wavelengths are located in the near infrared (NIR) or shortwave infrared (SWIR) region, e.g., 905 nm, 1064 nm and 1550 nm (Toth and Petrie 2018). Other wavelengths that have been used include green laser (534 nm), red laser (690 nm) and NIR at 785 nm. Because shorter wavelengths carry more energy increasing the risk of eye injuries, NIR or SWIR wavelengths are more commonly used. Generally, TLS systems employ only a single wavelength, but prototype sensors have been developed with dual-wavelength or even hyperspectral capabilities. The Salford Advanced Laser Canopy Analyser (SALCA) captures full-waveform of backscattered radiation at 1063 nm and 1545 nm wavelengths (Danson et al. 2014). Hakala et al. (2012) presented the first full waveform terrestrial lidar with eight tuneable channels in the visible and NIR region. Later, a hyperspectral lidar (HSL) with 32 channels has been developed (Sun et al. 2017), but these multispectral lidars utilize white supercontinuum laser as the laser source which due to eye-safety issues hinders their operability outside the laboratory environment. Thus far, no commercial TLSs with several wavelengths have been developed, but there is a commercial airborne lidar system with 532 nm, 1064 nm and 1550 nm wavelengths (Yu et al. 2017).

In addition to capturing the 3D structure of objects, TLS measures the intensity of the reflected light energy which correlates with the reflectivity of the object at the wavelength used in the TLS system. This enables the simultaneous mapping of object 3D structure and reflectivity at a very narrow band of the electromagnetic spectrum (Yu et al. 2017). The nature of the reflected light in lidar can be described by the radar equation (Eq. 1), which states that received power (P_r) is affected by transmitted power (P_t), aperture size (D), the optical efficiency of the lidar system (Q), the laser beam divergence (β), the atmospheric transmission losses (T), the range (R), and the backscattering cross-section of the target (σ):

$$P_r = \frac{P_t D Q}{4\pi\beta^2} T^2 \frac{\sigma}{R^4} \quad (1)$$

where σ is formed by target reflectance, geometry and the illuminated area. According to the equation, P_r is linearly dependent on transmitted power, aperture, optical efficiency and

target reflectance. The effect of atmospheric transmission losses is neglectable in TLS in forest environments where target distances rarely exceed 30 m. The effect of R is affected by the target shape due to spherical losses. Large surfaces, linear targets and blob-like objects all show a different response due to the changes in the backscattered irradiance field (Wagner et al. 2006). A large surface that fulfils the laser footprint entirely will show a fourfold decrease in P_r when R is doubled, whereas wires and leaves that cover the laser footprint partially will show a decrease of 8 or 16 times (Korpela 2017). Due to the varying shape of targets in tree canopies, range normalization is challenging for absolute radiometric calibration.

TLS intensity is affected by incidence angle of the laser beam. The Eq. 1 shows that P_r is in linear dependence with σ, which is comprised of target reflectance, geometry and illuminated area (Kaasalainen et al. 2011). The illuminated area increases as incidence angle increases for extended surfaces. Several studies have explored methods for incidence angle correction (Kaasalainen et al. 2011; Krooks et al. 2013; Tan and Cheng 2016). The correction methods require the calculation of incidence angle, which is usually done by fitting a plane to the 3D coordinates of the TLS data. This is challenging for small-leaved vegetation with few lidar hits per leaf requiring very high-resolution data, not to mention needle-leaved vegetation that does not necessarily fill a single laser beam footprint.

Multispectral lidar has the potential to overcome the aforementioned challenges. If two wavelengths are influenced by incidence angle in a similar manner, the ratio of the two should cancel the effect. This has been studied using HSL data with a small collection of leaf samples, concluding that the effect incidence angle on spectral indices (simple ratio and normalized difference index) is dependent on the internal structure and surface properties of leaves (Kaasalainen et al. 2016). In another study that included boreal tree species, both coniferous and deciduous, the conclusion was that lidar derived vegetation indices change with the laser incidence angle and that leads to systematic error that cannot be corrected with physical modelling for an individual point (Kaasalainen et al. 2018). Instead, larger areas should be used to average the geometric effects of varying incidence angles.

The relationship between raw lidar intensity measured by the instrument and target reflectance should be considered in the calibration of lidar intensity. Many TLS systems have shown a non-linear dependence between target reflectance and the measured intensity that should be corrected using external objects with known reflectance (Kaasalainen et al. 2005; Kaasalainen et al. 2009). Additionally, the effect of target moisture on lidar intensity should be acknowledged when developing methods using lidar intensity data (Kaasalainen et al. 2010).

The varying effect of distance on lidar intensity from different target geometries could be neglected with a lidar system using two or more wavelengths that are perfectly collinear and have same beam divergence, resulting in completely overlapping lidar footprints at multiple wavelengths. Then, based on Eq. 1 the effect of range would be the same on each wavelength enabling the calculation of spectral indices that are not affected by target distance. However, thus far, this topic has not been investigated.

1.4 Analyses of terrestrial lidar intensity in vegetation

Terrestrial lidar, or terrestrial laser scanning (TLS), can be used for very high-resolution modelling of vegetation structure to estimate e.g. tree structural attributes, above-ground biomass or canopy gap fraction (Danson et al. 2007; Calders et al. 2015; Liang et al. 2018). Traditionally, the utilization of TLS data has been based on the three-dimensional structure of the point clouds produced by TLS, since the instruments provide accurate range

measurements. However, recently the use of lidar intensity (i.e., the strength of the reflected light) has gained more attention in the science community due to its ability to retrieve information on the reflectivity of a target at the lidar wavelength (a very narrow band of the electromagnetic spectrum), in addition to capturing the 3D structure of the target. Many studies have investigated the radiometric calibration of lidar intensity, but the task has proven to be challenging for forest canopies which are characterized by complex shapes (Kashani et al. 2015; Korpela 2017).

The utilization of lidar intensity, or reflectance, is based on the effect of vegetation structure and biochemical properties on the reflectance of leaves, needles and vegetation canopies (Figure 3). Different biochemical components tend to affect the reflectance spectrum of leaves at a certain part of the electromagnetic spectrum, which can be employed for the assessment of the various components using narrow bands (Feret et al. 2008; Du et al. 2016). Models such as the PROSPECT leaf reflectance model can be used to estimate the effect of the variable of interest on reflectance spectra (Jacquemoud and Baret 1990; Feret et al. 2008).

The interpretation of lidar intensity in RS is generally based on statistical features that describe the value distribution and the shape of the intensity distribution. This process may be preceded by various calibration procedures of the measured intensity described earlier, and in the case of multispectral lidar data, the calculation of various indices, such as simple ratio or normalized difference index that describe the ratio of multiple wavelengths (Chen 1996; Gillies et al. 1997). In empirical modelling, the calculated features are then compared with a "ground truth" (e.g., measured structure or biochemical property), which is the gold standard in RS, in order to find relationships between measured lidar intensity and the variable of interest. Empirical models have been widely applied in lidar studies, e.g., for linking forest stand or tree-wise structural information with lidar measurements (Naesset 1997; Hyyppä et al. 2008).

The ability of TLS in describing vegetation structure accurately has raised interest in very high-resolution mapping of the biochemistry of plants. Thus, TLS intensity has been used to assess several biochemical components, such as the leaf photoprotective mechanism, chlorophyll content, crop nitrogen content, and leaf water content (LWC) using single-wavelength TLS (Eitel et al. 2010; Eitel et al. 2014; Magney et al. 2014; Zhu et al. 2015). These studies have found good agreement between the variable of interest and TLS intensity despite the early stage of TLS intensity adaptation in research.

Multispectral lidar has the potential to be especially suitable for the assessment of the biochemical composition of plants. As was shown earlier, leaf structure and various biochemical components of leaves have their own unique response in terms of reflectance throughout the electromagnetic spectrum. However, as can be seen in Figure 3, the responses may overlap. The employment of two wavelengths can assist in separating the effect of the variable of interest from a structural component. By using one wavelength inside the range of the spectrum where the structural component exhibits changes, while the second wavelength is located in a range that is sensitive to the variable of interest, it is possible to rule out the effect of the structural component inside the spectral range of the variable of interest.

Multi- and hyperspectral lidar has been used to assess rice and oat leaf nitrogen content and Scots pine shoot and rice leaf chlorophyll content (Nevalainen et al. 2013; Nevalainen et al. 2014; Du et al. 2016; Sun et al. 2017; Sun et al. 2018). These studies have shown that simultaneous retrieval of reflectance and structure at very high-resolution has high potential in the estimation of biochemical properties. However, these studies are mainly focused on small-scale laboratory tests with limited field applicability.

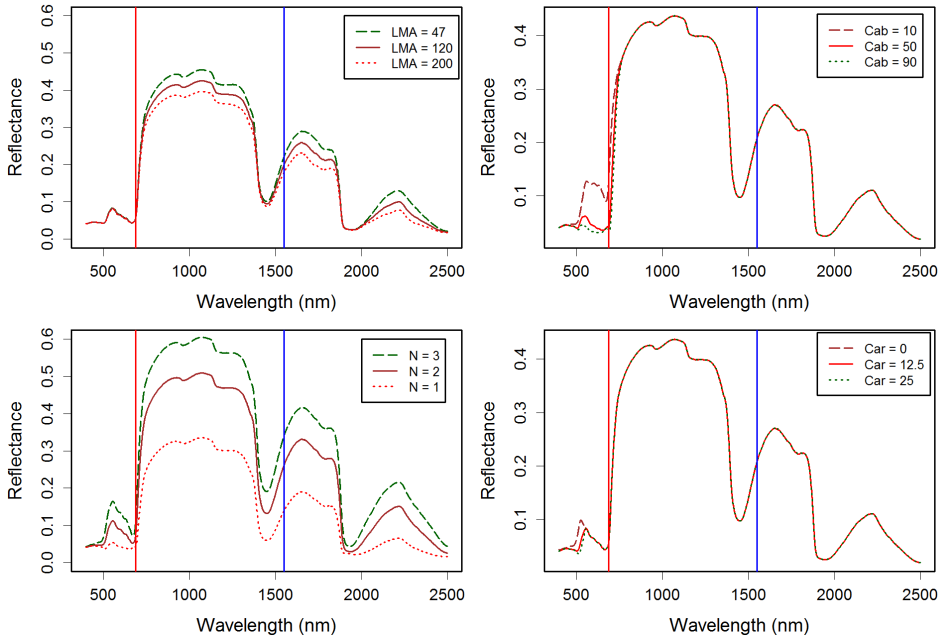

Figure 3. Reflectance spectra of a leaf with varying biochemical and structural parameters modelled with the PROSPECT-5 model by varying one model parameter while others were constants. Leaf mass per area (LMA), chlorophyll a+b content (Cab), leaf internal structure parameter (N) and carotenoid content (Car) was modelled. Vertical lines stand for laser wavelengths 690 nm and 1550 nm (Adapted from study II.)

The utilization of lidar intensity in estimating LWC has been preliminary investigated. The first to show the potential of dual-wavelength TLS intensity at 1064 nm and 1550 nm in estimating LWC was Gaulton et al. (2013). They showed promising results with single leaves of a variety of not-forest species, but the sample number was small. Zhu et al. (2015; 2017) used a single wavelength 1550 nm TLS to estimate LWC of deciduous species at single leaf and canopy-level in a laboratory environment using radiometric corrections to reduce the effect of incidence angle resulting in a good agreement between observed and predicted LWC.

1.5 Relationship between leaf water content and tree decline

LWC can be expressed using a variety of different metrics. They are based on the measurement of leaf fresh weight and leaf dry weight, which can be measured using a scale. Additionally, the leaf area may be measured for calculating the amount of water per leaf area, which is important in RS studies since the distribution of biochemical components per leaf area affects leaf reflectance (Feret et al. 2008). Leaf gravimetric water content (GWC) can be calculated with two different methods, which differ in the divider. The amount of water is divided by leaf fresh weight (GWC) using the following equation (Cheng et al. 2011):

$$GWC = \frac{FW-DW}{FW} * 100\% \quad (2)$$

where FW is the leaf fresh weight and DW is the dry weight. Equivalent water thickness (EWT) is calculated with the equation (Danson et al. 1992):

$$EWT = \frac{FW-DW}{A}\left(\frac{g}{cm^2}\right) \quad (3)$$

where A is the leaf area. Although the metrics are based on the amount of water within a leaf, EWT and GWC metrics do not necessarily correlate, but EWT is correlated with leaf thickness and leaf mass per area (Datt 1999).

Tree decline induced by a variety of pest insects, pathogens and drought can result in changes in LWC. Defoliation caused by the gypsy moth larvae (Lymantria dispar L.) has been shown to result in declined oak leaf quality including reduced GWC and increased dry matter content (Schultz and Baldwin 1982). There is evidence that leaf defoliators cause changes in plant secondary metabolites as a defence mechanism including the increase in leaf toughness, i.e. increased dry matter content (O'Reilly-Wapstra et al. 2012).

Drought directly affects the water status of trees when evapotranspiration is larger than precipitation (Bréda et al. 2006). The resulting drought stress can be observed also in the GWC that decreases with increasing water stress (Tucker 1980). GWC has been identified as a good indicator of water stress and it is related to water potential (Siddique et al. 2000). Sinclair and Ludlow (1985) have stated that GWC would be a better indicator of plant water status than water potential, which has been identified as a sensitive indicator of water stress (McCutchan and Shackel 1992).

The European spruce bark beetle (*Ips typographus* L.) has been identified as a disturbance resulting in significant decrease in EWT already in the early stages of infestation (Abdullah et al. 2018). The disturbance is caused by the combination of larvae that feed on the phloem of the trees and a blue stain fungal pathogen (*Endoconidiophora polonica*) that disturbs the flow of water within the xylem (Horntvedt et al. 1983). The blue stain fungi is able to kill healthy trees alone if inoculated in sufficient amounts (Horntvedt et al. 1983). The mountain pine beetle (*Dendroctonus ponderosae* Hopkins) has been shown to affect similarly the water balance of tree crowns (Skakun et al. 2003). It is also a pest insect which lays eggs under the bark introducing a blue stain fungus into the sapwood at the same time (Coops et al. 2006). The jack pine budworm (*Choristoneura pinus* Freeman) larvae causes defoliation in the upper part of the crown resulting in drying of the needles and in cases, widespread tree mortality (Radeloff et al. 1999).

LWC is a key measure also in estimating the ignition probability of forest fires (Chuvieco et al. 2004). In forest fire studies, LWC is often expressed as fuel moisture content (FMC), which is calculated by the same equation as GWC described above (Chuvieco et al. 2002). Thus, tree and forest decline that results in decreased FMC can lead to increased forest fire risk. While insect damaged timber may be usable for certain forest products, forest fires damage timber completely, cause massive CO_2 emissions and can jeopardize human lives and settlements as has been recently documented e.g. in California, U.S (Ramirez et al. 2018).

1.6 Aims and structure of this dissertation

This dissertation investigates multispectral terrestrial lidar data and evaluates its capability in detecting declined trees. Specifically, the dissertation studies the relationship between lidar

intensity and LWC, evaluates LWC as a tree decline indicator and investigates the capability of lidar intensity in detecting declined tree health of varying levels.

The primary aim of the dissertation was to develop a new RS method for the estimation of tree health condition by providing accurate LWC measurements using multispectral lidar intensity. The role of forests globally is crucial in the mitigation of climate change due to their ability to sequester carbon from the atmosphere. Information on the condition and health of forests is a key to be able to evaluate whether forests are acting as a source or a sink of carbon. Thus, the second aim was to enhance the understanding of the link between tree decline and LWC. By combining LWC measurements and other measures of tree decline, I aimed at evaluating multispectral lidar intensity information for the detection of tree decline.

The structure of this dissertation can be divided into three topics as follows: The first topic of the dissertation was dedicated to the development of a novel method for the mapping of LWC (Figure 4). First, the potential of multispectral lidar in the detection of drought related tree decline was studied (Study I). This was followed by an extensive leaf-scale study on the accuracy of EWT estimation using multispectral lidar with the most significant species in boreal forests (Study II). After this, the developed method was applied to Norway spruce seedling canopies to assess the accuracy of the method for live plants and study the response of EWT to varying drought treatments and the inoculation of a fungal pathogen (Study III). Finally, the applicability of the developed methods was tested with Norway spruce in a mature forest environment (Study IV).

The second topic of the dissertation was dedicated to investigating the relationship between LWC and tree decline for enhanced understanding of the usability of different LWC metrics in the detection of tree decline. This topic was based on the data acquired in two studies with different disturbances: a greenhouse study with Norway spruce seedlings (Study III) where drought and fungal pathogen treatments were applied and a study in a forest environment with mature Norway spruce infested by *I. typographus* (Study IV).

The third topic of the dissertation was dedicated to estimating the capability of multispectral terrestrial lidar in detecting tree decline by observing tree decline symptoms. First, the response of multispectral lidar intensity to different disturbance treatments was studied in a greenhouse environment with Norway spruce seedlings (Study III). This was followed by testing similar methods in the detection of varying tree decline caused by *I. typographus* in mature Norway spruce forest (Study IV).

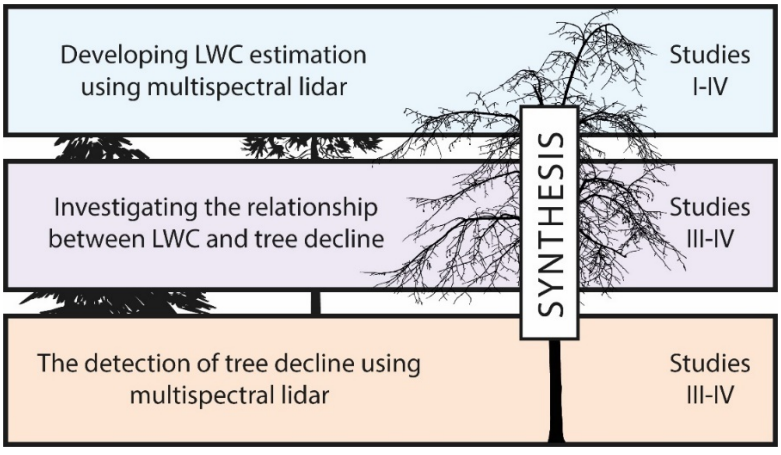

Figure 4. The topics of the dissertation and the corresponding studies.

2. MATERIAL AND METHODS

2.1 Experiment design

The studies in this dissertation were performed in various environments with different experiment setups (Figure 5). The conducted investigations have progressed from detailed small-scale measurements in the laboratory step-by-step towards tests in the field with mature trees. The study I was conducted in a laboratory setting where single trees (3-3.5 m height) were measured using HSL with the top of the canopy facing the scanner, simulating an airborne data acquisition (Table 1). The dataset consisted of nine Norway spruces (*Picea abies* L.) and nine Scots pines (*Pinus sylvestris* L.) that were measured with HSL from 3-meter distance before and after a drought treatment. The drought treatment was implemented by leaving the cut trees outside without a water supply for 12 days.

The study II was also based in a laboratory environment where single leaves and groups of needles were used as material. Five species important for forest and urban landscapes in Northern Europe were selected for the study: Norway spruce, Scots pine, Silver birch (*Betula pendula* L.), Norway maple (*Acer platanoides* L.) and Small-leaved lime (*Tilia cordata* L.). Single leaves and groups of needles were attached to black cardboard frames for TLS measurements, which was conducted as a time-series investigation as the leaves dried naturally. Each of the 101 leaf and needle samples was measured 12 times on average during

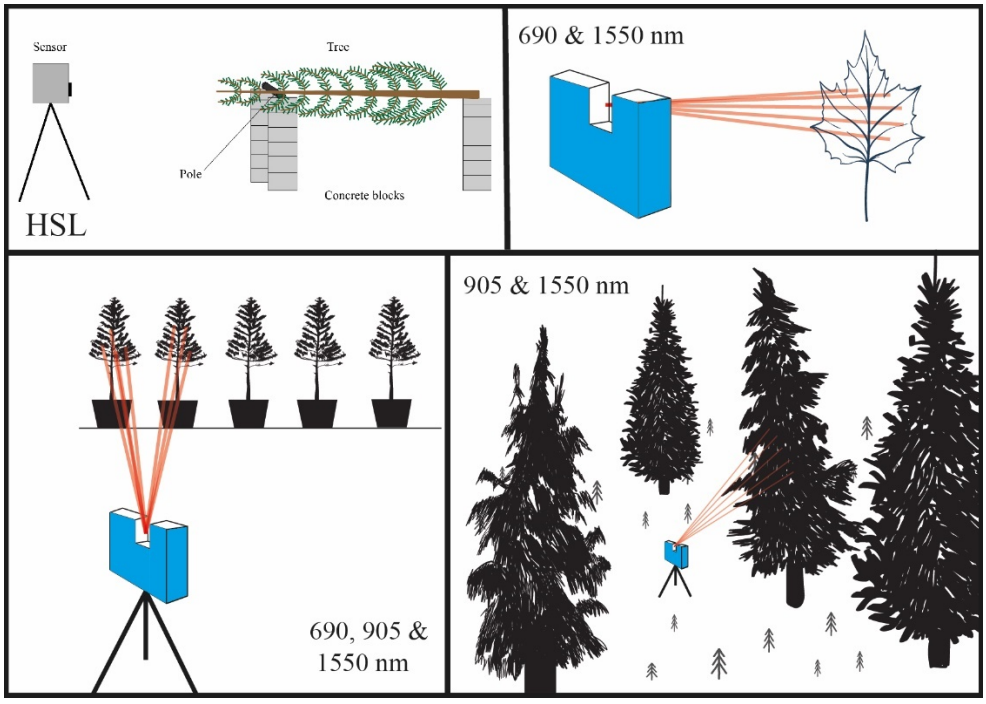

Figure 5. The different scales of the terrestrial lidar measurements used in the studies. Top left: study I, top right: study II, bottom left: study III and bottom right: study IV.

the experiment, resulting in a dataset with 1,180 data points including a measured reference EWT and measured lidar intensity at 1550 nm and 690 nm wavelengths.

The experiment in study III was implemented in a greenhouse with tree seedlings during 12 weeks between May and August 2016. A total of 145 Norway spruce seedlings of 2-years old was divided into different treatment groups to induce variation in LWC. Two kinds of disturbance were implemented: drought and inoculation with a fungal pathogen. The drought group consisted of four subgroups that had different watering regimes: 75%, 50%, 25% of normal irrigation and a group with normal irrigation until a complete stop of watering for three weeks. The pathogen group was inoculated with a fungal pathogen (*Endoconidiophora polonica*) that is associated with the European spruce bark beetle (*I. typographus*). Approximately 12 seedlings were randomly collected for TLS measurements and destructive sampling of EWT at eight time intervals.

The field measurements of study IV were conducted in the municipality of Ruokolahti in SE Finland in August 2017. There has been an on-going bark beetle infestation by *I. typographus* since 2010 in the study area affecting the condition of Norway spruce. The tree damage due to the infestation was mitigated by a cold summer in 2017, thus, the infestation symptoms were low and moderate within the area during data collection. The study area is characterized by mature Norway spruce forest that is mixed with European rowan (*Sorbus aucuparia* L.), European aspen (*Populus tremula* L.) and Silver birch (*Betula pendula* Roth.). A total of 33 Norway spruces were selected according to the infestation symptoms for further measurements of EWT, GWC and TLS. The infestation symptoms were classified in the field by experts based on the condition of foliage (defoliation, discoloration) and bark (resin flow, bark structural damage, bark beetle insertion holes) allowing the calculation of an attack score level. The attack level score was calculated by summing the symptom classifications. Then, based on the attack level score value, the trees were classified in groups of no infestation, low infestation and moderate infestation. The EWT and GWC measurements were done by sampling the canopy foliage at two heights using a shotgun.

2.2 Biochemical measurements

Biochemical measurements were done in studies II-IV for the investigations. LWC was measured based on leaf and needle samples in studies II-IV. The calculation of EWT requires leaf area measurements which were done using photointerpretation methods. In study II, the samples were photographed with a reference target with a known area and leaf area was segmented based on RGB values of the images (Easlon and Bloom 2014). A flatbed scanner

Table 1. Summary of the species, number of plants, scale and environment of each sub-study.

Study	Species	Number of plant samples	Scale	Environment
I	Norway spruce, Scots pine	18	Canopy-level	Laboratory
II	Norway spruce, Scots pine, Small-leaved lime, Norway maple, Silver birch	101	Leaf-level	Laboratory
III	Norway spruce	145	Branch-/canopy-level (seedlings)	Greenhouse
IV	Norway spruce	33	Canopy-level	Forest

was used in studies III-IV for scanning of the sample and the resulting image was segmented using the RGB values.

The fresh leaf and needle samples in studies II-IV were weighted immediately after sampling or lidar measurements using a precision scale. The samples were dried in 60°C for 48 h to measure dry weight. In studies II-IV, EWT was investigated. Studies II and IV investigated also leaf mass per area (LMA).

$$LMA = \frac{DW}{A} \quad (4)$$

where DW is dry weight and A leaf area. In study IV, GWC was also calculated (specified in the introduction section).

2.3 Terrestrial lidar measurements

Five different TLS instruments were used to measure tree and leaf samples in the studies. In the first study (study I), HSL was used, which sends white laser light using a supercontinuum laser source (Hakala et al. 2012). The HSL is capable of recording the full waveform of the returned lidar pulses at eight wavelengths located in the visible and NIR region (Table 2). The HSL is based on time-of-flight measurement for calculating the distance between the target and the scanner, and it is a prototype instrument for laboratory tests limiting its employment in the field. The HSL can measure multiple returns per lidar pulse.

The operability in the field and the range of wavelengths was limited in the HSL. Thus, in the following studies (II-IV), commercially available TLS instruments were used, which allowed field-operability and the utilization of longer wavelengths that are more sensitive to LWC. In study II, two commercially available TLS instruments were used: a Leica HDS6100 (Leica Geosystems AG, Heerbrugg, Switzerland) operating at 690 nm wavelength and a FARO X330 (FARO Europe GmbH & Co. KG, Korntal-Münchingen, Germany) operating at 1550 nm wavelength. In study III, three TLS instruments were employed: the Leica HDS6100, the FARO X330 and a FARO S120 operating at 905 nm wavelength. In study IV, two scanners were used: the FARO X330 and a Trimble TX5 (Trimble Inc., Sunnyvale, CA, USA) operating at 905 nm wavelength. The Trimble TX5 is essentially the same instrument with same technical specifications as FARO S120, but from a different brand. All the commercially available scanners mentioned above utilize phase-shift measurement technique for range determination. The selection of TLS instruments was based on theoretical assumptions and practical availability at the time of the investigation.

The technical specifications of the different scanners used in the studies are somewhat similar, except for the HSL, which is a hyperspectral time-of-flight instrument and can record full waveform. In the commercial scanners that were used in studies II-IV, the beam divergence is very similar (0.19 mrad, Leica: 0.22 mrad) and beam diameter at exit is 3 mm, except for FARO X330: 2.25 mm. The similar optical specifications resulted in similar viewing geometries since the beam diameter, i.e. lidar footprint, varied only slightly (5.1-6.3 mm) at a distance of 15 m. The commercial scanners produced discrete point clouds with xyz-coordinates and an intensity value recorded at 12-bits.

The TLS measurements were conducted from the same distance although several scanners were used in studies II-IV to avoid the effect of distance on the measured intensity. In study II, the scanners were placed next to each other, as close as was possible, facing the targets. In studies III-IV, the scanners were attached on the same tripod consequently. The boxing in the FARO and Trimble scanners was the same, thus, the TLS measurements were performed from the same position, although different scanners were used. Examples of the

point clouds of each study are visualized in Figure 6, where one can observe the high detail of the measurements and the slight difference in point density in each study. A reference panel with known reflectance was used in each TLS measurement. Three (study III) or four (study IV) external sphere targets were placed in the scanned scene to facilitate the registration of the point clouds.

2.4 Post-processing of lidar point clouds

Post-processing of lidar point clouds was required to separate the target of interest from the surroundings. In studies I-II, the area of interest was manually delineated from the point clouds, and no georeferencing of point clouds was required. Post-processing of the coordinates of the lidar point clouds into a common coordination system was necessary in studies III-IV to facilitate the point delineation process and the merging of the point clouds. Three (study III) or four (study IV) external sphere targets were placed in each scan for the co-registration of the point clouds into a common coordinate system. The point clouds in studies III-IV contained a lot of "ghost points" that are points in between targets (Balduzzi et al. 2011). The number of ghost points was reduced by applying a statistical outlier filter, which filters points that are far from other points. The distance threshold is calculated with the following equation:

$$MaxD = MeanD + nSigma * std, \quad (5)$$

where *MaxD* is the maximum distance of a point to be included, *MeanD* is the mean distance of the neighboring points, *nSigma* is a standard deviation multiplier threshold, and *std* is the standard deviation of the distance of the neighboring points.

To separate lidar intensity response from tree needles and bark or stem the point clouds were classified into needle and stem points in studies III-IV. The classification was done with manual segmentation in study III and automatically in study IV. The automatic classification

Table 2. Technical specifications of the lidar instruments used in the studies.

Laser scanner	Beam diver-gence (mrad)	Beam diameter at exit (mm)	Beam diame-ter at 15 m (mm)	Wavelength(s) (nm)	Intensity recording (DN)	Ranging error (mm)	Used in studies
Hyperspectral lidar	0.35	2	7.25	554.8, 632.5, 691.1, 725.5, 760.3, 795.0, 899.0, 1000.4	Full waveform	±12	I
FARO X330	0.19	2.25	5.10	1550	−2048 to 2033	±2	II, III, IV
Trimble TX5	0.19	3	5.85	905	−2048 to 2033	±2	IV
FARO S120	0.19	3	5.85	905	−2048 to 2033	±2	III
Leica HDS6100	0.22	3	6.3	690	-1228 to 2048	±2	II

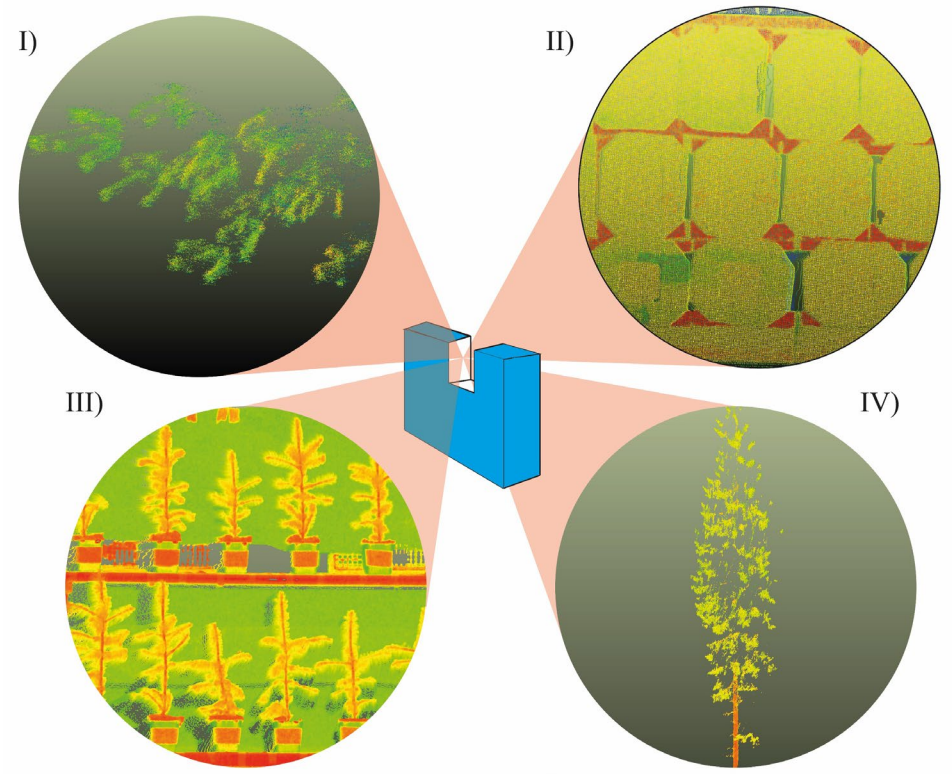

Figure 6. The point clouds of each study visualized. The cardboard frames can be seen in the point cloud of study II.

was based on multiscale dimensionality features, that were calculated using a training sample of 40,000 manually classified points (Brodu and Lague 2012). In study IV, the point clouds at 905 nm and 1550 nm wavelengths were merged point-by-point by calculating the nearest point.

2.5 Calibration of lidar intensity

Calibration of lidar intensity was required to reduce the effect of distance, incidence angle, cross-sectional geometry and instrument specific behaviour (Kaasalainen et al. 2009). The full waveform data in study I was processed using Gaussian function fitting and an external reference target to acquire backscattered reflectance values (Hakala et al. 2012). The raw intensity digital number values in the commercial scanners (used in studies II-IV) were converted into relative reflectance using empirically developed regression models between reflectance and raw intensity measurements (Kaasalainen et al. 2009). The empirical data consisted of three (studies II-III) or five (study IV) Spectralon (Labsphere, North Sutton, NH, USA) reflectance panels that were measured with the scanners and with an ASD FieldSpec Pro FR (Analytical Spectral Devices, Inc., Boulder, CO) field spectrophotometer. The FARO and Trimble scanners showed a non-linear relationship between raw intensity and reflectance, thus, a logarithmic model was applied in the conversion process (Figure 7) (Kaasalainen et

al. 2008). The Leica scanner showed a linear relationship allowing the utilization of a linear regression model. In all the studies, an external reflectance target was used to normalize for the effects of the ambient environment (e.g. temperature).

In study II, an incidence angle correction was applied on the intensity to correct for the curvy and wrinkled surface of the leaves (Figure 8). The incidence angle was calculated by finding a surface normal for each point. A plane was formed by finding the nearest points within a radius of 4 mm and fitting a plane to the points. The incidence angle was calculated for the fitted plane with the following equation:

$$\cos\alpha = \frac{\mathbf{P}\cdot\mathbf{N}}{|\mathbf{P}|*|\mathbf{N}|}, \quad (6)$$

where α is the incidence angle, **P** is the lidar beam vector from the TLS to the surface, and **N** is the surface normal vector.

An empirical scattering model that combines the Lommel-Seeliger law and the Lambert's cosine law was used to correct the incidence angle effect in study II (Kaasalainen et al. 2011). The correction was done with the following equation:

$$I(\varepsilon) = a(\omega, g)(1 - b(\omega, g)(1 - \cos\varepsilon)), \quad (7)$$

where I is backscatter intensity at angle ε, ω is the albedo and g the grain size of the material. The parameter b is a Lambertian component and parameter a is the intensity at zero incidence angle. The model parameters were evaluated visually from density scatterplots. The species of interest in studies III-IV was Norway spruce with needles, thus, an incidence angle correction was not applied.

The removal of specular (i.e. mirror-like) backscatter intensity was tested in study II to compensate for the different reflective properties of leaf surfaces. A model that is a mix of Lambertian and non-Lambertian reflectance was used to simulate leaf reflectance as follows (Poullain et al. 2016):

$$I = f\left(k_d \cos\alpha + 1\frac{(1-k_d)}{cos^5\,\alpha}e^{-\left(\frac{tan^2\alpha}{m^2}\right)}\right), \quad (8)$$

where I is the backscatter intensity, f is the backscatter intensity at normal incidence angle, k_d is the fraction of diffuse backscatter intensity, α is the incidence angle and m is the surface roughness parameter. The model parameters were visually estimated using density scatterplots of intensity and incidence angle to find the fraction of specular backscatter intensity.

Distance calibration of lidar intensity was conducted to reduce the effect of distance on measured intensity. The acquisition of TLS measurements was performed from a constant distance in studies I-III and no range correction were applied on the intensity. The TLS data in study IV contained various ranges and a range correction of the intensity was necessary. Both scanners, FARO X330 operating at 1550 nm and Trimble TX5 operating at 905 nm wavelength, showed a similar trend in the relationship between intensity and distance (Figure 9). The intensity showed a peak in near ranges followed by a positive slope towards longer ranges, which is a result of internal amplification in the scanner. The different amplification algorithms in different scanners complicate the utilization of intensity data since model specific correction parameters are required. The range correction was done using a polynomial model fitted between empirically acquired range and intensity measurements

(Tan and Cheng 2016). A reflectance panel was measured at 2-meter intervals from 3 m to 33 m distance and a 10-degree polynomial model was fitted to the data.

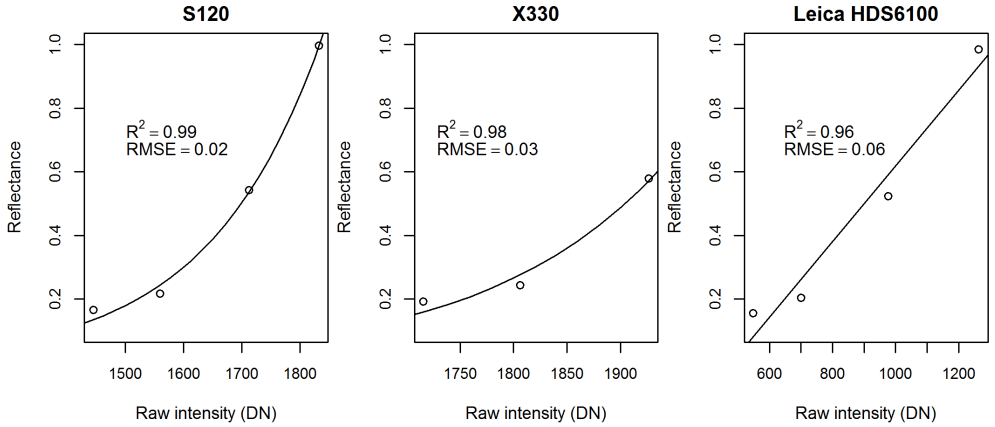

Figure 7. The relationship between measured raw intensity and measured reflectance of FARO S120, X330 and Leica HDS6100. (Figure adapted from study III.)

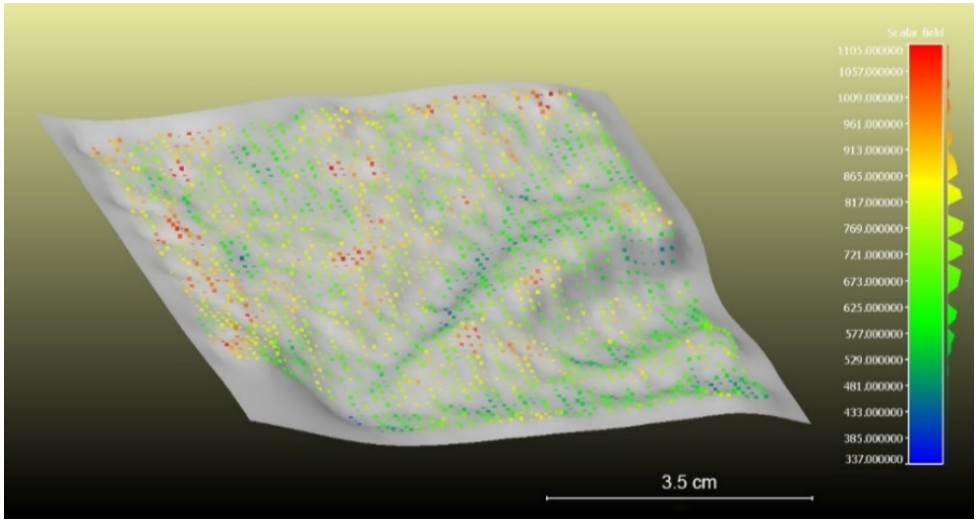

Figure 8. A sample of a Norway maple leaf measured with the FARO X330 with a constructed surface illustrating the curvy nature of the leaf surface. The colours represent raw intensity values. (Figure adapted from study II.)

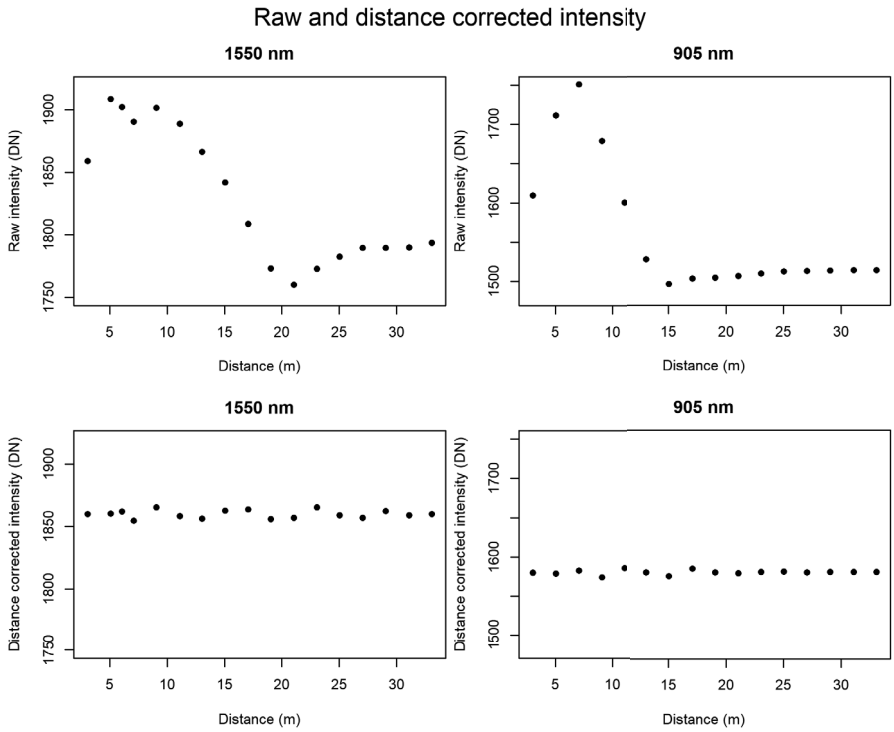

Figure 9. The relationship between intensity and distance at 1550 nm and 905 nm wavelengths before and after the distance correction. (Figure adapted from study IV.)

2.6 Lidar intensity metrics

Lidar intensity metrics are used to describe the measured intensity distribution to investigate the relationship between lidar intensity and the variable of interest. For each investigated point cloud representing a sample, a set of different intensity metrics was calculated (Table 3). They describe the intensity value distribution in different ways using statistics.

The statistical metrics that were used could be divided into two categories: value-based metrics and shape-based metrics. The value-based metrics (used in studies I-IV), such as mean, standard deviation (std), percentiles or quantiles, are dependent on the values of the intensity distribution, i.e. the success of the intensity calibration process is in direct relation to these metrics (Figure 10). The shape-based metrics (used in study IV), such as kurtosis, skewness or Shannon diversity index, are dependent on the shape of the distribution (e.g. how the value distribution compares to a normal distribution), but independent of the actual values in the distribution (Figure 11). Two distributions with different ranges and means can be the same in terms of skewness, for example. Thus, the intensity calibration process and its success in outputting comparable absolute reflectance does not affect the shape-based metrics as much as the value-based metrics.

The calculation of the intensity metrics was based on the intensity data at single wavelengths and calculated spectral indices. In study I, a normalized vegetation difference index (NDVI) (Gillies et al. 1997) was calculated based on wavelengths at 691 nm and 795

Table 3. List of intensity metrics, wavelengths used, and the units of interest for which the metrics were calculated.

Study	Unit	N	Wavelengths (nm)	Intensity metrics
I	tree	36	554.8, 632.5, 691.1, 725.5, 760.3, 795.0, 899.0, 1000.4	mean, min, max, std, quantiles
II	leaf	1180	690, 1550	mean
III	seedling / branch	145	690, 905, 1550	mean, min, max, std, percentiles 10, 20, 30…, 90
IV	tree (foliage and stem)	29	905, 1550	mean, min, max, std, percentiles 10, 20, 30…, 90, kurtosis, skewness, Shannon diversity index, range, density bandwidth, density

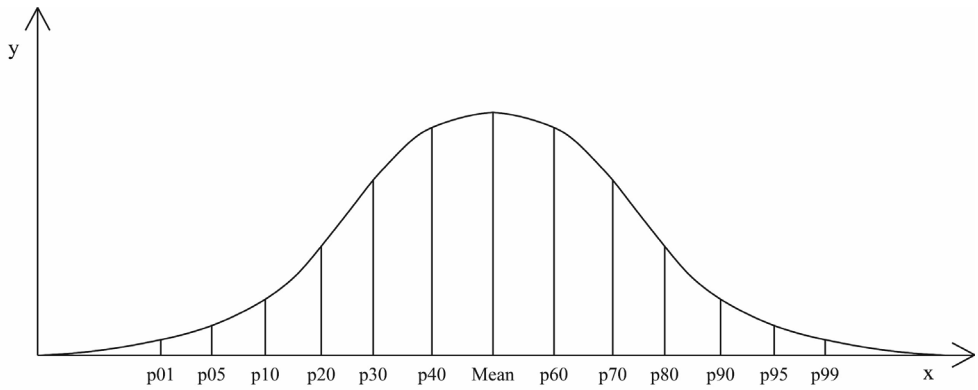

Figure 10. A set of value-based metrics visualized on a normal distribution. The letter “p” denotes “percentile”.

nm, and a modified water index (WI) (Peñuelas et al. 1997) was calculated based on wavelengths at 899 nm and 1000 nm. In studies II-IV, a simple ratio (SR) and a normalized difference index (NDI) was calculated based on the wavelengths in each study. In study II, these were referred as normalized laser difference index (NLDI) and laser ratio index (LRI). All possible combinations of wavelengths were used to calculate the spectral indices.

$$NDVI = \frac{I_{795} - I_{691}}{I_{795} + I_{691}} \quad (9)$$

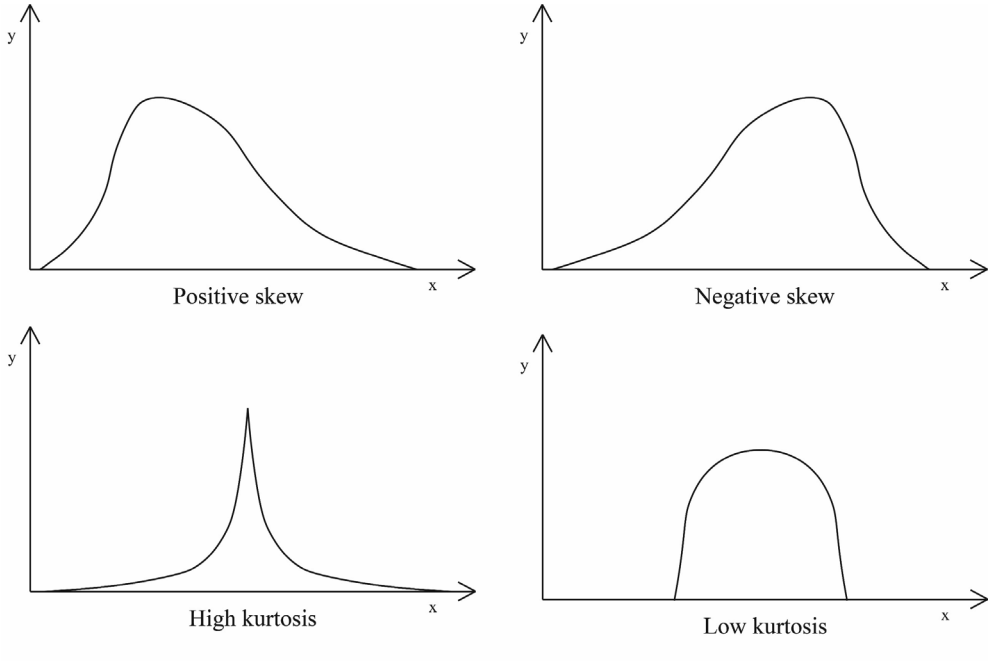

Figure 11. A set of shape-based metrics (skewness and kurtosis) visualized.

$$WI = \frac{I_{1000}}{I_{899}} \quad (10)$$

$$SR = \frac{I_{\lambda_1}}{I_{\lambda_2}} \quad (11)$$

$$NDI = \frac{I_{\lambda_1} - I_{\lambda_2}}{I_{\lambda_1} + I_{\lambda_2}} \quad (12)$$

The I in the equations denotes calibrated intensity and the footnote the wavelength used (λ_1 and λ_2 are the wavelengths of the scanners in studies II-IV). The HSL used in study I was able to record multiple returns; thus, the metrics were calculated separately for single, first and second returns. In studies II-IV, the metrics were calculated based on all the points in each point cloud since the scanners provided single return data.

2.7 Statistical methods

After obtaining the material that consisted of vegetation samples and a set of intensity metrics describing each sample, statistical methods were used to investigate their relationship. The statistical difference in the calibrated intensity between the drought-treated and fresh untreated trees in study I was evaluated using paired t-tests. Similar approach was used to determine the differences in LWC between the different infestation classes in study IV with unpaired t-tests. Linear simple regression models were employed widely in studies II-IV to

evaluate the dependency between calibrated lidar intensity metrics and LWC. In study IV, ordinal logistic regression modelling was used to evaluate the ability of individual intensity metrics in explaining different infestation symptoms (discoloration, defoliation, resin flow on stem) and the infestation class by comparing the statistical significance and McFadden pseudo R^2 (equation 14) of the models. Similarly, simple linear regression models were developed between attack level score, LWC metrics and the intensity metrics as predictors to compare the predictive power of each intensity metric. In addition, multiple regression models were used to assess the ability of intensity metrics in explaining LWC and attack level score (i.e. infestation severity). The coefficient of determination (R^2) (equation 15) with cross-validation was used to evaluate the goodness-of-fit and the ability of the predictors in explaining the independent variable. Root mean square error (*RMSE*) (equation 16) and *RMSE* % (equation 17) were used to evaluate the accuracy of the predictive models.

$$McFadden\ pseudo\ R^2 = \frac{d0-d}{d0} \tag{13}$$

$$R^2 = 1 - \frac{\sum_i (y_i - \hat{y}_i)^2}{\sum_i (y_i - \bar{y})^2} \tag{14}$$

$$RMSE = \sqrt{\frac{\sum_{i=1}^{n} (y_i - \hat{y}_i)^2}{n}} \tag{15}$$

$$RMSE\ \% = 100 * \frac{RMSE}{y_{max} - y_{min}} \tag{16}$$

where *d0* is the deviance of a null model, *d* is the deviance of the model, n is the number of observations, y_i is the observed value for the measurement i, $\hat{y}_i$ is the predicted value for the measurement i, $\bar{y}$ is the mean of the observed data, y_{max} and y_{min} are the maximum and minimum of the observed data, respectively.

The multiple regression models in study IV were developed with a stepwise algorithm and evaluated using adjusted (Adj.) and predicted (Pred.) R^2 to prevent overfitting of the models. The model selection was done using the Schwarz Bayesian information criterion, which penalizes for model complexity (Schwarz 1978). Additionally, variance inflation factor was calculated for the models to evaluate and prevent multicollinearity between predictor variables. The dependencies between biochemical components and infestation symptoms in study IV were evaluated using Pearson's correlation coefficient, when both variables were continuous, and Spearman correlation was used for variables with an ordinal scale. The ability of lidar intensity metrics in classifying infestation class was evaluated with linear discriminant analysis with a two-class (not infested, infested) and a three-class scheme (no, low and moderate infestation). The intensity metrics were chosen based on the comparison of intensity metrics ability to explain different infestation symptoms. A maximum of three variables were chosen in the linear discriminant analysis. The classification accuracy of the model was assessed using leave-one-out cross-validation since the low number of samples did not allow the creation of a separate data set. All the statistical analyses were conducted within the R software package (R Core Team 2013).

3. RESULTS

3.1 Leaf water content mapping: method development (studies I-IV)

In this first part of the results section, I discuss the results of the method development of LWC mapping, which was one of the main themes of this dissertation. The development of the methods begun with a simple test in study I, where the potential of HSL in detecting drought-induced reflectance changes in the canopies of single trees was assessed. It was shown that HSL was able to detect significant differences after the drought treatment using a NDVI derived from the 795 nm and 691 nm wavelengths. The difference was more pronounced using first or single returns. The drought induced alterations in spectral reflectance were more apparent in the NIR spectrum than in the visible wavelengths (Figure 12). However, the instrument was not capable of measuring lidar intensity at longer wavelengths in the SWIR region (> 1000 nm), which is more susceptible to variation in LWC. One disadvantage of HSL was that it is a laboratory instrument not suitable for measurements in the field. Thus, further investigations were required to assess the accuracy of multispectral lidar in quantifying LWC with instruments that operate in the SWIR region (1100-3000 nm) and could be operated in the field.

The leaf reflectance spectra of varying EWT was simulated using a leaf-level reflectance model (PROSPECT-5) in study II to determine suitable wavelengths for LWC mapping (Figure 13) (Feret et al. 2008). It was shown that LWC affects leaf reflectance in wavelengths above 1200 nm and the greatest range of variation, and thus, sensitivity to LWC, was observed around the 1500 nm wavelength. The selection of available wavelengths in TLS instruments is limited, but the 1550 nm wavelength is used in many, e.g. in FARO X330, which was available for further investigations. Thus, FARO X330 with 1550 nm wavelength was tested for estimating changes in LWC, which was accompanied by a Leica HDS6100 operating at 690 nm wavelength located at the red-light spectrum that showed constant reflectance with changing LWC.

After assessing the potential of multispectral lidar in detecting drought induced changes, the accuracy of the method in estimating LWC was investigated at leaf-level using 1550 nm and 690 nm wavelengths (Study II). The relationship between EWT and the lidar intensity was studied using simple regression modelling. Strong correlations between lidar intensity and EWT were found for each species (R^2 = 0.61-0.86). The NDI and SR indices did not show significant improvement over 1550 nm wavelength in the deciduous species but did for the conifer species (R^2 of 0.48-0.53 vs. 0.61-0.69), likely due to the more complex geometry of the coniferous targets. A very strong relationship between EWT and NDI was found by pooling all species together (R^2 = 0.93) (Figure 14). The calibrated lidar intensity was further processed to remove the effect of incidence angle the fraction of specular backscatter intensity. However, it was found that the additional correction processes did not affect the result significantly, likely due to the constant angle of the samples in relation to the scanner position.

Further investigations of simulated leaf-level spectra gave more insights of the effects of leaf structure on reflectance. By using leaf reflectance simulations, it was shown that the 1550 nm wavelength is sensitive to leaf internal structure, which is not apparent at 690 nm wavelength. Thus, it was concluded that multispectral lidar at the investigated wavelengths can accurately measure EWT at leaf-level in a controlled setting, but the selection of wavelengths was suboptimal due to the inability of 690 nm wavelength in normalizing the variation in the internal structure of leaves that affects reflectance at 1550 nm. Also, LMA was found to significantly ($p<0.0001$) correlate with 1550 nm wavelength adding uncertainty

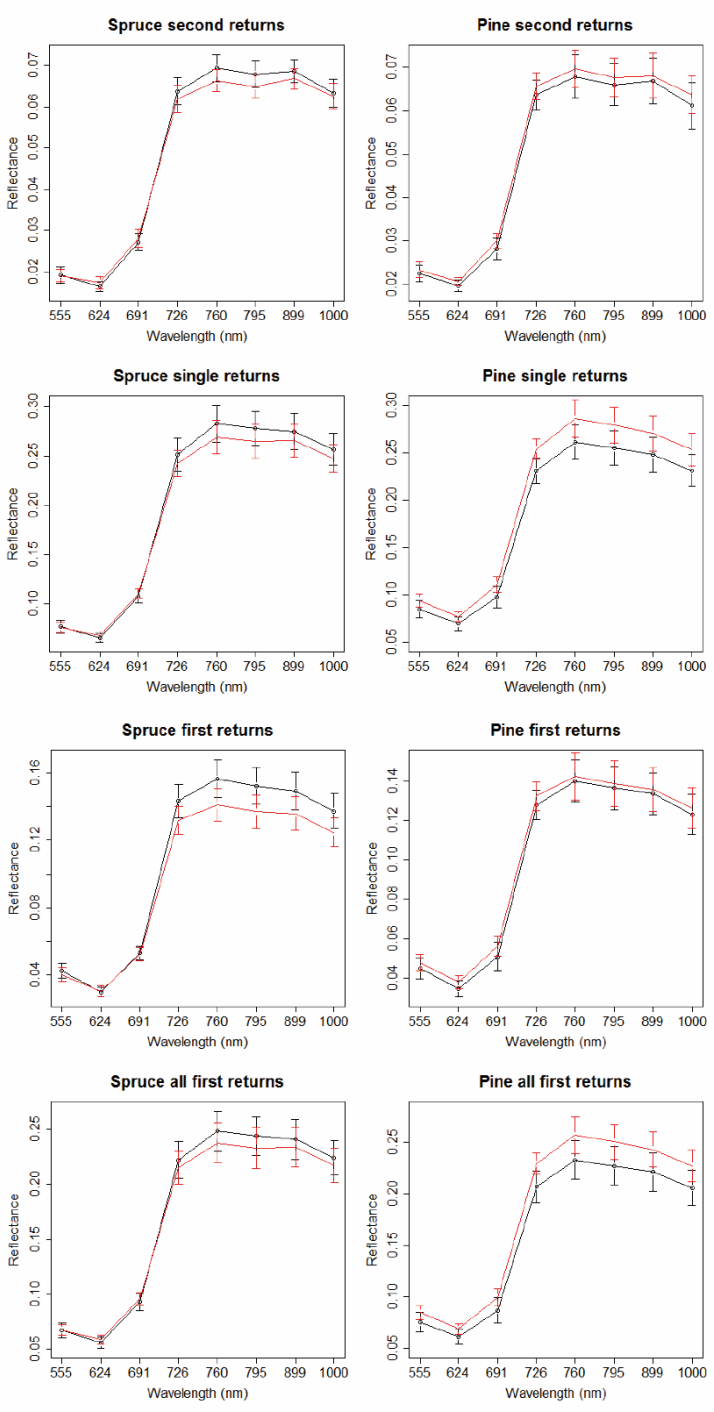

Figure 12. Reflectance of fresh (black lines) and drought-treated (red lines) trees. The line is the mean reflectance and the bars represent their standard deviations. (Figure adapted from Study I.)

to the reliable estimation of EWT. Since the measurements were done as a time-series, the variability of LMA was not an issue in the data set (i.e. each sample with single LMA value was measured multiple times). However, LMA is likely to vary in natural environments increasing uncertainty in EWT estimation. Therefore, the suitability of the method for the estimation of EWT with live plants was investigated in study III.

The method that was developed in study II to estimate LWC was tested with live Norway spruce seedlings in study III. To consider the conclusions made in study II about the optimal selection of wavelengths, a third TLS instrument was employed operating at 905 nm wavelength (in addition to 1550 nm and 690 nm). The 905 nm wavelength is sensitive to the internal cell structure and density of leaves (i.e. LMA) according to the simulations conducted in study II. It was found that the lidar intensity metrics could explain 89% (R^2) of the variation in EWT using an NDI calculated from 1550 nm and 905 nm wavelengths (Figure 15). This was significantly better than metrics calculated from the combination of 1550 nm and 690 nm (R^2 = 0.82) or the 1550 nm wavelength only (R^2 = 0.79). The segmentation of leaf and stem points improved the results for the single wavelength data, but not for the NDI. The calculated NDIs from the segmented stem points showed also strong linear relationships with EWT (R^2 = 0.66–0.75). Based on the results of conifer species in studies II and III, a conclusion was made that using a spectral index calculated from two wavelengths can reduce the effect of varying incidence angles and varying shape of the receiving area.

After conducting studies on estimating LWC with multispectral lidar in controlled environments the investigations were taken into the field to test the method in a mature forest environment. In study IV, the estimation of LWC, that was measured as EWT and GWC, was investigated at tree-level. Simple linear regression models were developed between EWT, GWC and individual intensity metrics showing that kurtosis of both 905 nm and 1550

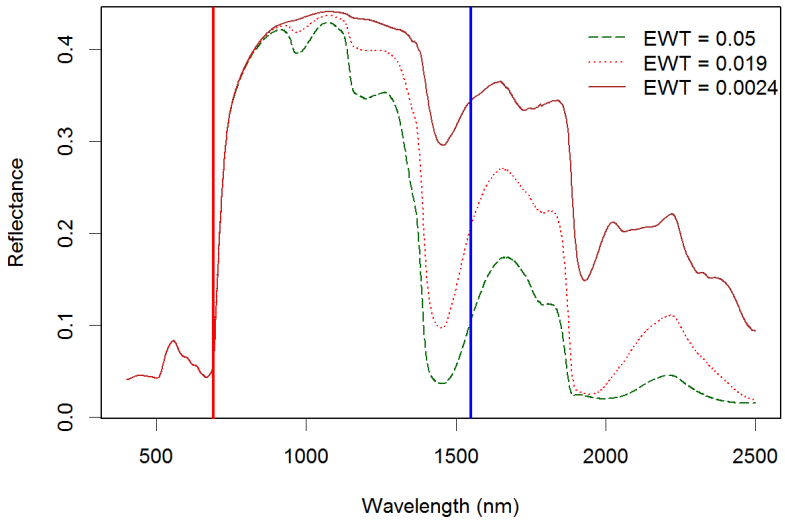

Figure 13. Reflectance spectra of a leaf with varying LWC, expressed in terms of EWT, simulated with the PROSPECT-5 model. All other model parameters were kept constant. (Figure adapted from study II.)

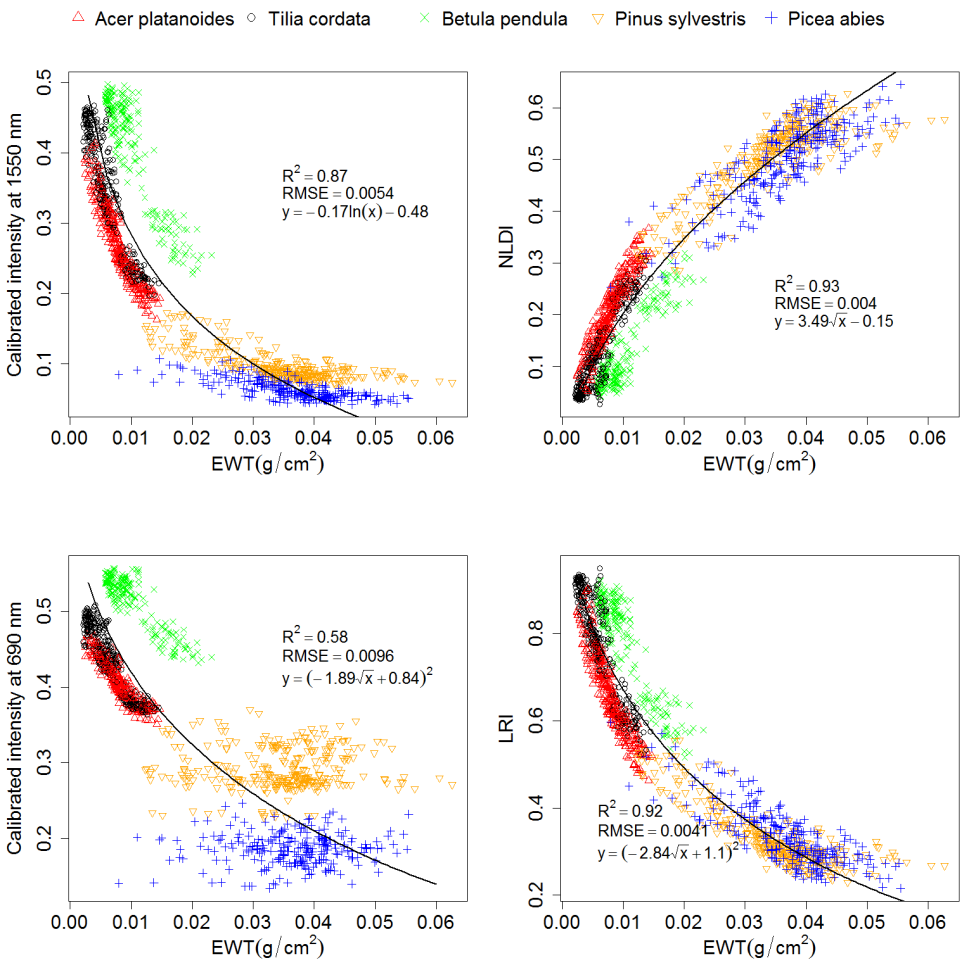

Figure 14. The relationship between EWT and calibrated intensity at 1550 nm, 690 nm and calculated spectral indices: NLDI and LRI. (Figure adapted from study II.)

nm wavelength were among the best predictors for EWT (R^2=0.33). Significant relationships (R^2=0.34–0.38) between the mean and percentiles of NDI measured from the stem and GWC was found indicating that the moisture content of bark is linked to canopy water content. The developed multivariate regression models explained 68% and 48% of the variation (Adj. R^2) in EWT and GWC, respectively (Figure 18). The variables chosen by the stepwise algorithm were based on canopy intensity metrics for EWT and on stem intensity metrics for GWC. The intensity metrics that were chosen to the multivariate regression models were mostly based on the NDI and 1550 nm wavelength value distributions, supporting the results from the previous studies.

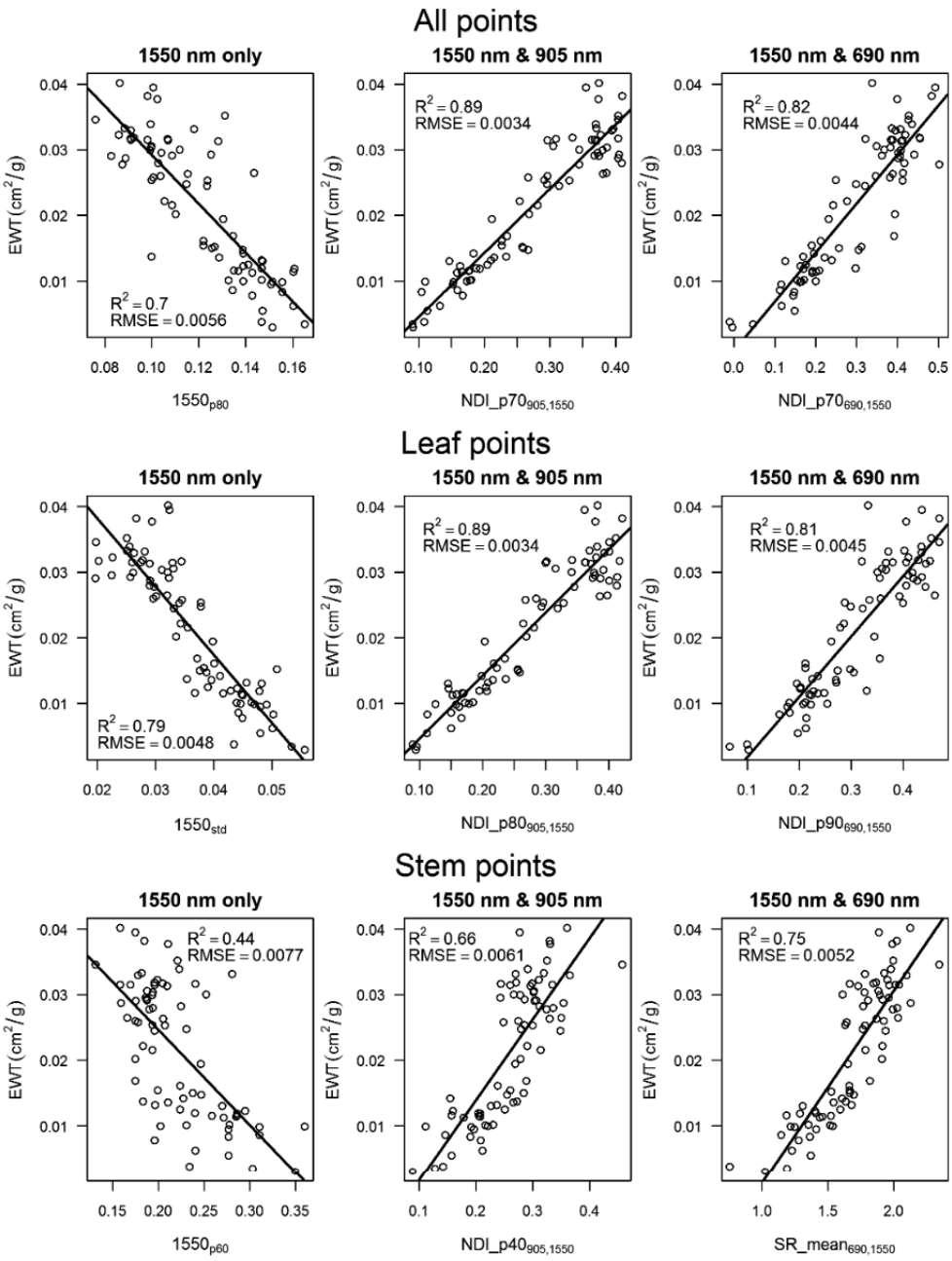

Figure 15. The relationship between intensity metrics from all, leaf and stem points and EWT in study III. (Figure adapted from study III.)

3.2 Effects of various disturbances on leaf water content (studies III & IV)

The second part of the dissertation was focused on understanding biochemical changes induced by tree decline and investigated LWC as an indicator of tree decline. More specifically, this part aimed at enhancing the understanding of the link between tree decline and LWC by studying trees with varying types of decline (Table 4).

The first study that investigated this theme in this dissertation was conducted in a controlled environment with seedlings that were exposed to different disturbances. In study III, the effect of drought on LWC was investigated by exposing Norway spruce seedlings to drought of varying intensities. The effect of drought was verified by measuring growth, which showed significant differences between the treatment groups (i.e. groups with different watering schemes) and was linearly negative with the intensity of the drought. The effect of drought on LWC was significant but mixed. On average, the less water the seedlings received, the smaller the LWC expressed as EWT was, but the differences between the groups were small and they overlapped. Thus, no significant differences within a certain measurement time were observed between the groups. The number of seedlings was small at each measurement time, hindering the statistical significance though. As the experiment went on and further reductions in the irrigation amount were made to intensify the drought treatment, EWT decreased significantly. It seemed however, that the greatest reduction was apparent only when the seedlings were close to mortality due to the lack of water. This is likely due to hydraulic failure in the xylem from cavitation resulting in halted flow of water from the roots to the needles that can result in plant death (Barigah et al. 2013).

A group of seedlings were inoculated with a pathogen blue-stain fungus that is associated with *I. typographus*. The response of EWT to the inoculation of *E. polonica* was a rapid decrease in the seedlings that showed infection symptoms (Figure 16). Most of the infected seedlings lost at least 50% of the EWT compared to uninfected seedlings during 2-3 weeks after inoculation. The change could be observed also visually as the new soft growth of needles wilted. About 50% of the inoculated seedlings were able to resist the pathogen and did not exhibit infection symptoms, which can be observed in Figure 16 with many seedlings not exhibiting a clear decline in EWT. Despite the inoculation, some of the seedlings did not exhibit any signs of infection even after 60 days.

Table 4. A summary of the disturbance types causing tree decline in studies III and IV.

Disturbance type	Primary or secondary disturbance	Study
Drought	Primary	III
Endoconidiophora polonica	Primary	III
Endoconidiophora polonica	Secondary (associated with *I. typographus* infestation)	IV
Ips typographus	Primary	IV

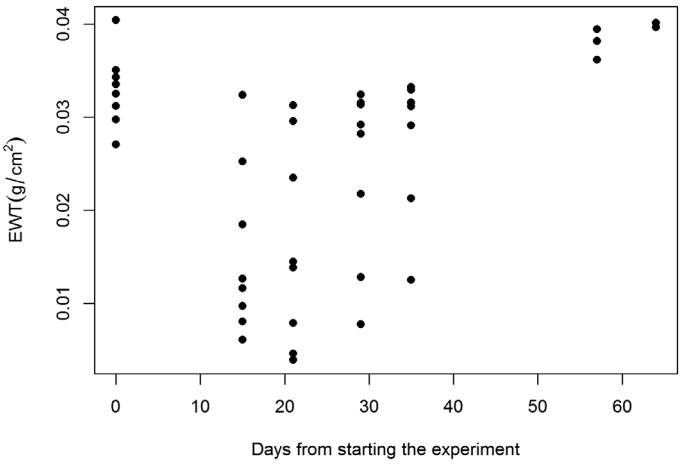

Figure 16. Changes in EWT after inoculation with *E. polonica*.

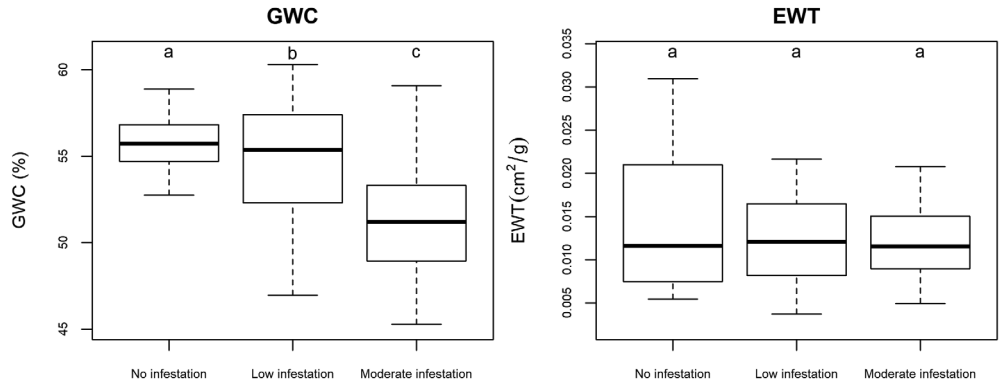

Figure 17. Boxplots of GWC and EWT in no infestation, low infestation and moderate infestation groups. Different letters on top of the boxes indicate significant difference at $p<0.05$ -level. (Figure adapted from study IV.)

The second study that contributed to studying the link between tree decline and LWC was study IV and it was conducted in a mature Norway spruce forest that showed various levels of infestation by *I. typographus*. The infestation was characterized by low to moderate damage with green-attack trees infested by *I. typographus*, which did not exhibit visual signals of tree decline, and trees with moderate damage including yellowing and defoliation of the crown. The trees were divided in three classes: not infested, low infestation (including green-attack) and moderate infestation. A significant decrease in GWC was detected in all the infestation classes, but no significant differences were found in EWT (Figure 17). EWT was shown to correlate very highly with leaf mass per area (LMA) ($r = 0.93$), and significantly with the height of the needle sample ($r = 0.34$). These results indicate that EWT varies due to local illumination conditions since LMA has been shown to be positively

correlated with daily photon irradiance, i.e. needles that receive more light have larger LMA and thus larger EWT due to the high correlation in the dataset (Poorter et al. 2009). EWT has been shown to decrease due to green-attack of *I. typogrpahus* but the samples in the study were taken from sunlit branches in the top of canopy, which is likely to decrease the variation in EWT measurements (Abdullah et al. 2018).

The different measures of LWC showed to behave differently with increasing infestation severity. GWC was identified as a suitable indicator of tree decline for *I. typographus* infested Norway spruce, but GWC and EWT did not correlate due to the relative insensitivity of GWC to varying LMA. There was no significant correlation between GWC and LMA ($r = -0.20$) indicating that GWC is a more independent measure of LWC, which is not affected by LMA. GWC was shown to correlate significantly ($p<0.05$) with the field measured indicators of tree decline: defoliation, discoloration, bark resin flow and bark beetle insertion holes. Structural bark damage was the only tree infestation symptom which did not show significant correlation with GWC. Of all the observed infestation symptoms, GWC was the most affected by the discoloration of the crown indicating that discoloration (i.e. changes in pigment content and chlorophyll) and GWC are correlated. Significant decreases in GWC were detected between all the infestation classes: not infested, low infestation and moderate infestation were separated ($p<0.05$). The relationship between the attack level score and GWC showed to be linearly negative. None of the tree decline indicators correlated significantly with EWT.

3.3 Detection of tree decline (studies III & IV)

The third aim of the dissertation was to investigate the capability of multispectral lidar in detecting tree decline. In study III, different disturbances were imposed to induce tree decline in Norway spruce seedlings. Drought treated seedlings showed lower growth rates, but the variation in LWC was relatively small until the drought was very severe. The detection of tree decline was based on lidar estimated LWC; thus, the detection was only possible after very severe drought.

The seedlings, which were inoculated with *E. polonica* in study III and showed infection symptoms, resulted in a rapid decrease in LWC. The decrease was clearly detectable using the developed linear regression model of LWC and a simple threshold could be used to separate the declined seedlings from the healthy ones.

Study IV was focused on the detection of tree decline in a mature spruce forest environment. Observed symptoms of tree decline (resin flow, canopy discoloration and defoliation) showed to significantly affect lidar intensity at both 905 nm and 1550 nm wavelengths. Discoloration of the crown affected the intensity metrics most significantly according to ordinal logistic regression models developed between bark beetle infestation symptoms and individual intensity metrics. On average, the 905 nm wavelength explained the severity of infestation symptoms slightly better than the 1550 nm wavelength, but the differences were small between the two wavelengths. The multivariate regression models that were developed to predict the attack level score using lidar intensity metrics explained 50% (Adj. R^2) of the variation in the attack level score (Figure 18). The discrimination between non-infested and infested trees was possible using a simple threshold allowing for the early detection of *I. typographus* infestation before visible discoloration of the tree crowns. The early detection was enabled by the ability of the intensity metrics in detecting the resin flow. From figure 18, one can observe how the infestation classes are aligned across the LWC metrics. A relationship between infestation severity and GWC can be observed but regarding EWT, the infestation classes are dispersed along the EWT values quite randomly.

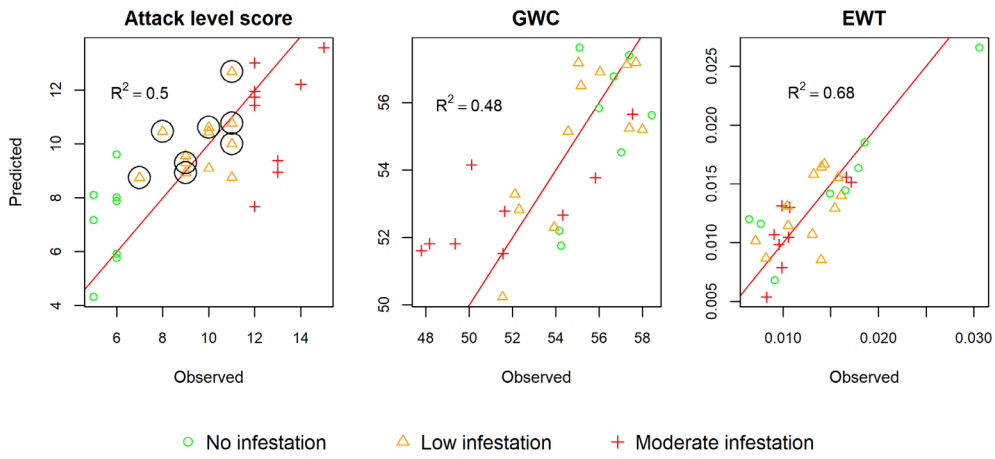

Figure 18. Observed vs. predicted values of attack level score, GWC and EWT obtained with multiple linear regression models. Circled points in the attack level score plot are green attack trees with no discoloration of the crown. Adjusted R^2 values are reported within the plots. (Figure adapted from study IV.)

Linear discrimination analysis was used to test the classification of infestation classes using lidar intensity metrics. The results showed that NDI and 905 nm wavelength metrics resulted in a 66% overall accuracy with three classes (no, low and moderate infestation). The classification accuracy of low and moderate classes was low resulting in a poor overall classification accuracy. A test with a two-class scheme with not infested and infested classes showed that a better accuracy was achieved (90% overall accuracy). The producer's accuracy for the no infestation class was 75% in both classification schemes. The intensity variables that were selected as classifiers were largely based on the distribution of 905 nm wavelength and NDI. The range of 905 nm of the stem was selected for both classification schemes indicating that the detection of resin flow on the stem contributed to the early detection of bark beetle infestation.

4. DISCUSSION

4.1 Leaf water content as a tree decline indicator

In this dissertation, the use of LWC as a tree decline indicator was examined. It was shown that LWC can vary significantly already in the early stages of bark beetle induced tree decline. However, there are significant differences in the LWC metrics that can be used. GWC showed to be sensitive to early tree decline while EWT did not vary significantly even in the moderate infestation class. It should be noted that the LWC measurements of each tree were comprised of two samples at different heights; thus, the sampling intensity may not be sufficient to detect significant differences in EWT due to the large variation of EWT within mature Norway spruce trees. EWT was affected by the location of the sampled branch in the canopy and was strongly correlated with LMA, which was found to significantly affect 1550

nm wavelength and calculated indices with 690 nm wavelength. These results raise a question: How accurately EWT can indicate leaf water status and tree decline if it is strongly linked to leaf structural properties that change over time and depend on local environmental conditions? If EWT is dependent on local illuminance conditions similar to LMA (Poorter et al. 2009), tree canopy position in relation to other trees is affecting EWT. Tree decline events are generally subtle in nature and forest managers need early information for decision making. The detection of small differences is complicated, if the natural variability of the tree decline indicator is large.

The drought treatments in study III showed little effect on EWT. EWT decreased significantly only after severe drought. The results were acquired in a controlled environment with Norway spruce seedlings. The generalization of the results to a natural forest environment is challenging. As was shown in study IV, mature trees can have large variation in EWT even within a single tree. Seedlings have more homogeneous canopies and environmental conditions, such as illumination, were constant between the seedlings. Therefore, it is difficult to draw conclusions of the effects of drought on more mature trees that have grown in varying conditions. The seedlings showed significant decrease in length growth with increasing drought intensity, but otherwise they showed no visual symptoms of decline. It could be due to the young age of the seedlings, that they are able to adapt to the lower irrigation amounts more easily than mature trees. Previous studies have shown that Norway spruce is less affected by drought in terms of basal area growth at a younger age (Kohler et al. 2010). The evapotranspiration from the small seedling canopies is less than from the large surface of mature tree foliage, allowing the seedlings to cope with a relatively broader range of irrigation amounts.

The seedlings that were inoculated with *E. polonica* in study III showed a rapid and significant decrease in EWT. The infected seedlings showed also visual symptoms of wilting. *E. polonica* damages the water transportation cells in the xylem and effectively blocks the flow of water to the canopy. *E. polonica* is a fungal species that lives in symbiosis with *I. typographus*. The bark beetle helps the fungi to relocate and the fungi assists the bark beetle in damaging the host tree for successful reproduction of the bark beetle (Brignolas et al. 1998). It is likely that *E. polonica* was one of the major factors causing the tree decline symptoms also in the test forest in study IV. Based on the experiments, *E. polonica* can cause rapid tree decline that is observable with LWC measurements.

A range of studies have investigated the reflectance properties of trees and its relation to tree decline. Skakun et al. (2003) used satellite-based observations to detect mountain pine beetle damage red-attack damage and found that a wetness index separated the healthy and declined forest areas with relatively good accuracy, supporting the use of LWC as a tree decline indicator. Higher resolution satellite-based RS data has been shown to be able to detect red crowns due to mountain pine beetle damage using a ratio of red and green reflectance, which was compared to a wetness index provided by the Landsat satellites (Coops et al. 2006). Immitzer et al. (2014) tried to use high-resolution satellite RS data to separate healthy, green-attack and dead trees with Norway spruce, resulting in overall classification accuracy of around 70%. However, there was significant overlap in the spectral response of the healthy and green-attack trees. Senf et al. (2015) found that both the mountain pine beetle and the western spruce bud worm reduced the wetness of the forest measured with Landsat satellites, also supporting the findings in this thesis that LWC is a suitable indicator for detecting tree decline.

Based on the field data with mature Norway spruce trees, it can be concluded that GWC is a more sensitive and robust indicator of tree decline and it should be preferred over EWT in measuring and detecting tree decline. Certainly, the tree species and the causes of tree decline are limited in this dissertation; thus, generalization of the results over a variety of

species and sources of decline is limited. However, as Norway spruce is one of the most important species economically in Europe and one the most widely planted spruces, there is potential for significant societal impact in developing tree decline indicators for this species (Schlyter et al. 2006). The mapping of GWC using RS methods is generally more challenging than EWT, because leaf reflectance is affected by leaf area (Feret et al. 2008). However, if GWC is more stable and varies less, as was shown in this dissertation, the absolute measuring accuracy requirement is less than for EWT for detecting significant differences.

The high correlation between LMA and EWT questions the applicability of EWT in describing leaf and canopy water status in Norway spruce. If the local illumination conditions or the developmental stage of needles affect EWT, how such variation could be considered to detect changes caused by tree decline? This is a difficult task and would require more information complicating the retrieval of tree decline estimates using EWT as a proxy. TLS could enable such approaches with detailed 3D information but future a more direct approach would be to further develop the estimation of GWC in future studies.

4.2 Measuring leaf water content with multispectral lidar

A variety of scales was investigated for the estimation of leaf and needle EWT (Table 5). The studies started from single leaves and groups of needles, then moved on to seedlings in study III and finally to mature Norway spruce trees in study IV. Based on the results, it was evident that multispectral TLS can estimate EWT at high accuracy in controlled environments where environmental conditions, plant material and scanning angles are relatively constant. The results showed that an NDI calculated from 905 nm and 1550 nm estimated EWT with the highest accuracy of the investigated wavelengths. Similar results have been obtained with other species also in controlled indoor environments (Zhu et al. 2017; Elsherif et al. 2018). The absolute measurement accuracy of EWT varied between different leaf structures deciduous species showing a higher measurement accuracy than coniferous species. This is likely due to the more uniform geometry of the leaf target resulting in less variation and error in the lidar intensity measurement. The shape of needles in coniferous species results in a more complex target geometry increasing the amount of multiple scattering (Korpela 2017). NDI seemed to be able to partially reduce the effect of multiple scattering since the greatest improvements in EWT estimation (compared to 1550 nm wavelength) were shown for coniferous species.

The application of the LWC measuring method in a forest environment was not as successful as the develop regression models explained EWT only moderately compared to the previous studies conducted in controlled environments. This may result from the following reasons. The reference EWT measurements may have been inadequate, as the trees exhibited larger variation in EWT than expected. If the independent variable contains a lot of error in the regression models, the accuracy of the predictors in explaining the independent variable (EWT in this case) is difficult to estimate. The classification of points into stems and needles may have too much error. As the scanning was conducted with single scans, the point density and detail in structure is lower than using multiple scans to reconstruct a tree. The point classification was based on dimensionality features, thus, the detail of structure in the point clouds directly affects the accuracy of the classifiers. Or then more likely, the distance calibration of lidar intensity lacks in correcting for the distance effect from needles due to varying relationship between lidar intensity and distance with different target geometries. The results from study IV in the field showed that the shape of the intensity distribution (measured with metrics such as kurtosis or skewness) provided the greatest predictive power in terms of EWT estimation. The fact that the strongest relationship between leaf GWC and

Table 5. Summary of the results of the estimation of EWT.

Study	Type of material and treatment	Type of model or test	Best predictors	R^2
I	Cut trees (3 m height) left with no watering	Paired-sample t-tests	725–1000 nm, NDVI	-
II	Cut leaves left to dry in cardboard frames	Linear regression models	NDI (690 & 1550 nm)	0.93
III	Seedlings with different watering regimes and pathogen inoculation	Linear and multiple regression models	70^{th} and 60^{th} percentiles of NDI (905 & 1550 nm)	0.89–0.91
IV	Mature trees with varying bark beetle infestation symptoms	Linear and multiple regression models	kurtosis of 905 nm and 1550 nm and range of NDI	0.16–0.68

intensity measurements was found from the percentiles and the mean of NDI of the stem, which is a less complex target, gave further evidence that the canopy measurements contain error that is caused by multiple scattering and varying receiving area.

The estimation of GWC from canopy intensity measurements failed and only very weak correlations could be observed. This could partly be due to intensity calibration issues, but also result from the effect of leaf area on measured intensity since EWT showed a significant relationship with lidar intensity. However, a strong correlation between measured intensity of the tree stem and GWC was observed indicating that bark moisture content is linked to canopy GWC. Further indication of the link between tree stem and leaf moisture content was given in study III where the segmented seedling stem points showed a strong relationship with EWT. No bark moisture content measurements were conducted in the studies, so this conclusion remains on a speculative level and requires further investigations.

4.3 Using multispectral lidar intensity in tree decline detection

The ability of multispectral lidar in detecting tree decline was based on slightly differing approaches in studies III-IV. The rapid decline in EWT due to fungal pathogen inoculation and the high correlation of EWT and multispectral lidar intensity in study III enabled the detection of pathogen induced tree decline. The drought induced tree stress was less observable by lidar intensity due to relatively constant EWT until very severe drought was present. The investigations conducted in the field (study IV) showed that also other tree decline symptoms beside declined LWC can be detected from the lidar measurements. Both the multivariate regression models and linear discriminant analyses revealed that the detection of resin flow on the tree stem was a significant factor in detecting declined trees in addition to canopy intensity metrics at both 905 nm and 1550 nm wavelength. Multivariate regression models developed between multispectral intensity metrics and bark beetle infestation severity showed moderate agreement with a selection of intensity metrics from both the stem and the canopy. The classification of infested and not infested trees showed an overall accuracy of 90%, but it should be noted that there was no separate dataset for an independent accuracy assessment. The classification accuracy of infested trees into low and

moderate infestation was low. Therefore, multispectral TLS showed potential in providing objective tree decline measurements, but the low number of sample trees (n=29) and a single study area limit the generalization of the results. Thus, further investigations are required to confirm the results and assess the accuracy of the method in different forest sites with varying structural and spatial properties.

Regarding the distance correction of intensity, there are few matters of to consider. The shape of leaves varies in deciduous species, but the physical process of lidar backscattering is relatively homogeneous as the leaves form a continuous surface where most lidar hits are covered entirely by the target. As with coniferous species, there is large variation in the shape of the target illuminated by the laser beam. A single lidar pulse can illuminate a single or several needles with its footprint, the gap between the needles can vary and the neighboring needles may have a small distance difference to the scanner. The result is very diverse in terms of the shape and geometry of the surface that causes a reflection of light that is captured by the TLS instrument (Figure 19). Ultimately, this causes varying decay with distance and random variation in the lidar intensity measurement, which is complicated to take into account (Kaasalainen et al. 2018). However, the utilization of several wavelengths, i.e. multispectral lidar, seems to reduce this error, as the estimation of EWT was significantly improved in the three studies (II-IV) by using a spectral index. Similar results have been obtained previously by studying the dependency between incidence angle and spectral indices (Kaasalainen et al. 2016).

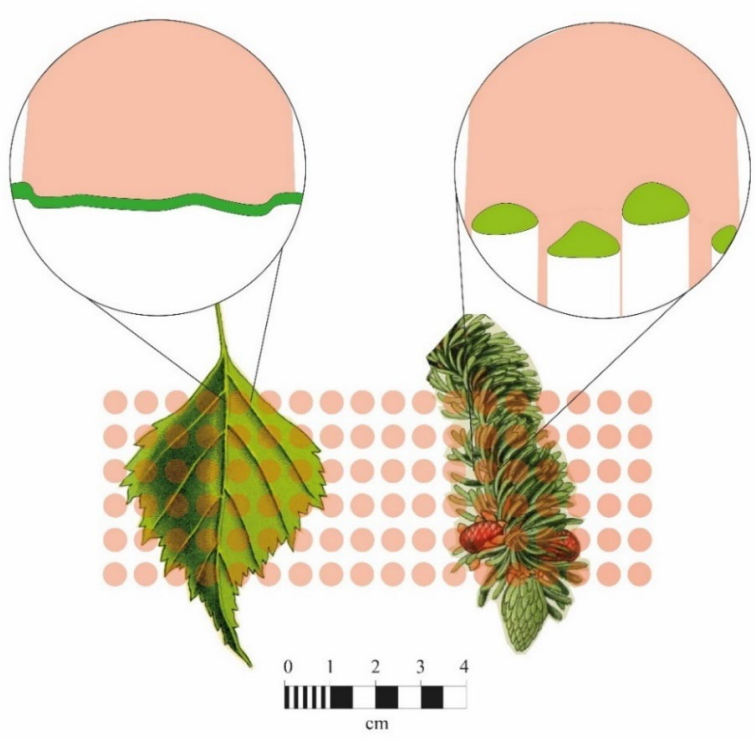

Figure 19. Schematic figure of the differences in the surface that is illuminated by laser light in deciduous and conifer species. The laser beam diameter is 5.3 mm in diameter in the figure which is equal to 12 m distance with the FARO S120 scanner.

The distance calibration of lidar intensity can be an ill-posed problem for tree canopies, especially for conifer species for which it is more difficult to determine how the lidar beam has illuminated a target (Hovi 2015). Since the distance effect on lidar intensity is dependent on the shape of the illuminated area, a new calibration method is required for accounting this effect (Korpela 2017). So far, the calibration models that have been developed for TLS are largely based on the assumption that the target surface is large enough to cover the lidar beam entirely. While this assumption holds for many deciduous species, coniferous species mostly have needles that are smaller in width than the laser beam diameter at target, resulting in different backscattering properties and stronger decay of the returning light with distance. Hence, different parts of tree crowns (stems, needles) need appropriate distance correction algorithms for absolute and comparable calibration of lidar intensity between targets of different shapes. The shape of tree crowns and individual branches vary according to site index and position in relation to other trees further complicating the modelling. However, the dense point clouds produced by TLS have sufficient structural detail for such an approach to be possible. Developing such calibration procedures would be a major step towards the utilization of lidar intensity as a robust tool for classifying e.g. tree health, biochemical properties and wood quality. Another approach to tackle the distance calibration challenge, would be to develop a new multispectral lidar sensor that have perfectly collinear lidar beams at several wavelengths with the same beam divergence resulting in same lidar footprint at multiple wavelengths. In theory, if the wavelengths are similarly affected by distance, the calculated ratios of two wavelengths would not be affected by the distance calibration issue.

The imperfections in the calibration procedure discussed above seem not to prevent entirely the detection of declined trees with multispectral TLS. As was shown in study IV, the metrics that are based on the shape of the intensity distribution showed statistical power in explaining infestation symptoms and LWC. The multivariate regression models explained only a moderate proportion of the variation in measured tree decline, but more importantly, the detection of early stages of bark beetle infestation showed potential. The intensity metrics were better able to discriminate not infested and infested trees than the infestation severity within the infested trees (low and moderate infestation). Thus, the lidar intensity could exhibit tree decline despite the shortcomings of the intensity distance calibration. Similar approaches have been used for measuring forest structural attributes with image point clouds from unmanned aerial vehicles using only the shape-based metrics of the upper canopy layer (Giannetti et al. 2018). Similarly to the results acquired in study IV, significant increase around 905 nm has been found due to severe mountain pine beetle damage and in the green attack stage of bark beetle attack using spectrophotometer measurements (Ahern 1988; Cheng et al. 2010).

The detection of tree decline using multispectral lidar could be improved with an optimal selection of wavelengths. According to Abdullah et al. (2018) the most significant changes were observed between 730 nm and 1370 nm region between not infested and bark beetle green attacked Norway spruce. In that study, significant differences ($p<0.05$) were also observed in SWIR region between 1430 nm and 1500 nm, which is outside the 1550 nm wavelength used in this dissertation. On the other hand, SWIR region between 1420 nm and 1850 nm wavelength has shown significant differences in green attacked tree foliage in another study (Abdullah et al. 2018). Other bands that have been found suitable for early detection of bark beetle infestation include 1310–1390 nm and 1000–1050 nm regions (Cheng et al. 2010). Engelmann spruce (*Picea engelmannii* (Parry ex Engelm)) that was in the green attack stage showed increased reflectance in SWIR region from 1450 to 2500 nm while NIR region showed no alterations (Foster et al. 2017). Early mountain pine beetle did not show significant changes around 970 nm wavelength, but did for 1200 nm wavelength (Niemann et al. 2015). Based on these studies, the optimal selection of suitable wavelengths

seems not clear as results from different studies are somewhat conflicting and likely there are species- and site-specific differences in foliage response to bark beetle infestation. Also, the timing of data collection slightly differs between studies affecting the ability to detect the progressive changes in leaf chemistry that are induced by growth and accumulation of dry material within cells.

Further investigations are required to determine the optimal wavelengths to detect different tree decline symptoms such as resin flow on tree stem or discoloration of the crown. Other decline symptoms should be linked to the spatial structure of tree canopies such as defoliation that has been accurately estimated using TLS (Huo and Zhang 2019). A combination of optimal wavelengths and spatial features that can estimate individual symptoms of tree decline at high accuracy could yield considerably better estimates of tree decline. However, the calibration of lidar intensity data needs to be developed further to exploit the full potential of the intensity measurements. Furthermore, the available selection of wavelengths is generally limited in multispectral lidar instruments, which can hinder the utilization of optimal wavelengths.

Passive hyperspectral imaging methods can utilize a wider range of wavelengths and have shown capabilities in detecting tree decline caused by bark beetle infestation (Lausch et al. 2013; Näsi et al. 2015). The 3D structure of tree canopies can be reconstructed from geolocated images using structure from motion methods enabling 3D point clouds with spectral information (Näsi et al. 2018). These methods are based on the passive detection of reflected sun energy and thus are sensitive to illumination conditions and shadowing. Hyperspectral imaging has shown that it can discriminate severely declined or dead trees with good accuracy but generally the early detection of subtle changes in the canopy has been challenging (Fassnacht et al. 2014; Näsi et al. 2018). A recent study, however, has successfully detected bark beetle green attack stage with Sentinel-2 satellite imagery in an area with large areas of green attacked trees and future improvements can be expected as methods and technologies develop (Abdullah et al. 2018).

4.4 Outlook for future method development

There are several matters that should be investigated to take the developed methods further. First, the scaling up of tree decline measurements from individual trees to compartment or even regional scale using multispectral lidar should be studied. The use of airborne multispectral lidar in detecting declined trees for mapping larger areas needs to be investigated in future studies to examine its capabilities. Questions, such as, what kind of pulse density or how many lidar measurements per tree are needed for tree decline detection? The viewing geometry and detail of measurements varies between airborne and terrestrial measurements and how this affects the detection of decline? How the multisensory airborne lidar instruments can measure LWC from above? It could be expected that the top of the canopy has less variability in LWC than the whole tree facilitating the measurements, since a significant correlation between sampling height and EWT was found in study IV. Also, EWT has shown significant differences already in the green attack stage when only sunlit needles from top of the canopy were sampled, but no differences were found in study IV (Abdullah et al. 2018). Another question is if the airborne sensors can observe early tree decline. The lidar measured stem characteristics were found useful with TLS but the stem is not measurable from above canopies. Another way to scale up would be using the TLS measured tree decline as a reference for satellite measurements. Sentinel-2 data has shown potential in detecting early forest decline but its potential is not well known due to the young age of the satellite products (Abdullah et al. 2018). Secondly, the detection of decline with

more species and causes of tree decline needs to be studied to assess the full potential and accuracy of multispectral lidar in tree decline detection. There are many species that affect trees similarly (e.g. *I. typographus* and *D. ponderosae*); thus, conclusions for wider applicability can be made, but the effects of defoliators and bark beetles on tree physiology, for instance, are different.

Considering sensor development and intensity calibration, there are several questions that need to be addressed. The varying effect of distance on lidar intensity due to target geometry requires for a novel correction method or other data-driven approaches that could diminish the effect of this issue. Could sensors with collinear lidar beams at several wavelengths with same beam divergence and similar optical properties be developed? And what are their capabilities in improving the utilization of intensity data? A ratio of two wavelengths could help removing the problem if both wavelengths are similarly influenced by distance. There are research lidar instruments that utilize white supercontinuum laser source, but these are dangerous to be used in the field due to eye-safety issues because of the high-power laser. Collinear lidar beams have potential in reducing the effects of target geometry, varying receiving area and incidence angle on the measured intensity but the topic has not been thoroughly investigated. Lidar intensity with airborne lidar data has shown potential in detecting tree decline in terms of defoliation also with single wavelength intensity, but the feasibility of using it has been drawn back due to complications in calibrating the intensity data (Kantola et al. 2013).

Point cloud technologies are increasingly used in forest monitoring and forest resource assessments and new sensors are being developed decreasing the cost of data collection (Eitel et al. 2016; Liang et al. 2018). Lidar sensors have been deployed on a variety of different platforms ranging from backpacks to all-terrain vehicles and from drones to satellites (Lin et al. 2011; Kukko et al. 2012; Flener et al. 2013; Qi and Dubayah 2016). In the future, technological and navigational advancements will allow for more efficient and thorough lidar measurements compared to using TLS which is time consuming considering the requirements of forest planners. Time-series of 3D forest structure measurements will create new possibilities to refine forest inventories and measure e.g. growth at unpreceded detail (Eitel et al. 2016). Tree growth in relation to its leaf area index is an important indicator of tree decline; thus, new ways to measure forest health will be enabled in the future (Waring 1983). Time-series data of lidar derived LWC measurements could also enhance the understanding of tree LWC dynamics and provide new means for detecting declined trees. This dissertation has shown that multispectral lidar can provide accurate tree decline information with a one-time measurement. Future studies should focus on utilizing this information on a wider scale with point cloud ecosystems that span from terrestrial to airborne and even spaceborne measurements to help decision makers in managing forests in a sustainable manner in the face of climate change and enhance the understanding of tree decline processes at different scales.

5. CONCLUSIONS

New methods for detecting and estimating tree decline were developed and evaluated in this dissertation. The condition and health of World's forests are jeopardized due to climate change. All the ecosystem services forests provide, such as carbon storage and uptake, renewable material, income for rural livelihoods, edibles and other non-timber forest products and outdoor activities, are directly affected by the health and condition of forests.

There is large uncertainty in the resilience of forests under changing climate and one of the key questions to be able to solve this problem is how to measure tree decline objectively in an efficient manner. This dissertation was dedicated to solving this problem in the field.

The first aim of this dissertation was to develop a method for the estimation of LWC using multispectral lidar. The developed methods showed that accurate estimates of LWC can be achieved in controlled environments where measurement distance and plant material are relatively constant. The estimation accuracy of LWC in the field was hindered by lidar intensity distance calibration, which was less successful for tree canopies.

The second aim was to investigate the relationship between LWC and tree decline. Results from the LWC measurements of bark beetle infested trees showed that LWC metrics differ significantly. GWC was sensitive to early tree decline while EWT showed no changes due to tree decline but correlated highly with LMA. Norway spruce seedlings that were inoculated with a blue-stain fungus showed a rapid decline in LWC while drought-treated seedlings showed constant levels of LWC until very severe drought was induced. These results gave new insight to the utilization of LWC as a tree decline indicator.

The last and third aim was to evaluate multispectral lidar in detecting declined trees. It was found that several indicators of tree decline affect lidar intensity significantly allowing the detection of the decline using multispectral TLS, but further studies are required for a reliable accuracy assessment in forest environments. In a forest environment, the measurement of tree decline should be linked to tree infestation symptoms of the stem and the canopy accounting for both changes in LWC and structural variability due to e.g. defoliation. By using multispectral TLS intensity, it was possible to detect early signs of tree decline and classify bark beetle infested trees with fair accuracy. Intensity distance calibration methods require further development to improve the accuracy of the methods and to allow robust comparison of different datasets.

This work outlines the feasibility and the limits of multispectral TLS in the detection of declined trees and points towards future research topics that should be addressed for a more robust utilization of lidar intensity and improved detection of tree decline. It has been shown before that TLS can measure the structure of trees with high detail and now the detection of tree decline and LWC mapping can be added to the vast list of possibilities this technology provides.

REFERENCES

Abdullah, H., Darvishzadeh, R., Skidmore, A. K., Groen, T. A. and Heurich, M. (2018). European spruce bark beetle (*Ips typographus*, L.) green attack affects foliar reflectance and biochemical properties. International Journal of Applied Earth Observation and Geoinformation 64: 199-209. https://doi.org/10.1016/j.jag.2017.09.009.

Abdullah, H., Skidmore, A. K., Darvishzadeh, R. and Heurich, M. (2018). Sentinel-2 accurately maps green-attack stage of European spruce bark beetle (*Ips typographus*, L.) compared with Landsat-8. Remote sensing in ecology and conservation. https://doi.org/10.1002/rse2.93.

Ahern, F. (1988). The effects of bark beetle stress on the foliar spectral reflectance of lodgepole pine. International Journal of Remote Sensing 9(9): 1451-1468. https://doi.org/10.1080/01431168808954952.

Allen, C. D., Breshears, D. D. and McDowell, N. G. (2015). On underestimation of global vulnerability to tree mortality and forest die-off from hotter drought in the Anthropocene. Ecosphere 6(8): 1-55. https://doi.org/10.1890/ES15-00203.1.

Anderson, L. O., Malhi, Y., Aragão, L. E., Ladle, R., Arai, E., Barbier, N. and Phillips, O. (2010). Remote sensing detection of droughts in Amazonian forest canopies. New Phytologist 187(3): 733-750. https://doi.org/10.1111/j.1469-8137.2010.03355.x.

Auclair, A. N. (1993). Extreme climatic fluctuations as a cause of forest dieback in the Pacific Rim. Water, Air, and Soil Pollution 66(3-4): 207-229.

Balduzzi, M. A., Van der Zande, D., Stuckens, J., Verstraeten, W. W. and Coppin, P. (2011). The properties of terrestrial laser system intensity for measuring leaf geometries: A case study with conference pear trees (*Pyrus Communis*). Sensors 11(2): 1657-1681. https://doi.org/10.3390/s110201657.

Barigah, T. S., Charrier, O., Douris, M., Bonhomme, M., Herbette, S., Améglio, T., Fichot, R., Brignolas, F. and Cochard, H. (2013). Water stress-induced xylem hydraulic failure is a causal factor of tree mortality in beech and poplar. Annals of Botany 112(7): 1431-1437. https://doi.org/10.1093/aob/mct204.

Bosteels, D. and Searles, R. A. (2002). Exhaust emission catalyst technology. Platinum metals review 46(1): 27-36.

Bréda, N., Huc, R., Granier, A. and Dreyer, E. (2006). Temperate forest trees and stands under severe drought: a review of ecophysiological responses, adaptation processes and long-term consequences. Annals of Forest Science 63(6): 625-644. https://doi.org/10.1051/forest:2006042.

Brignolas, F., Lieutier, F., Sauvard, D., Christiansen, E. and Berryman, A. A. (1998). Phenolic predictors for Norway spruce resistance to the bark beetle *Ips typographus* (Coleoptera: Scolytidae) and an associated fungus, Ceratocystis polonica. Canadian Journal of Forest Research 28(5): 720-728. https://doi.org/10.1139/x98-037.

Brodu, N. and Lague, D. (2012). 3D terrestrial lidar data classification of complex natural scenes using a multi-scale dimensionality criterion: Applications in geomorphology. ISPRS Journal of Photogrammetry and Remote Sensing 68: 121-134. https://doi.org/10.1016/j.isprsjprs.2012.01.006.

Calders, K., Newnham, G., Burt, A., Murphy, S., Raumonen, P., Herold, M., Culvenor, D., Avitabile, V., Disney, M. and Armston, J. (2015). Nondestructive estimates of above-ground biomass using terrestrial laser scanning. Methods in Ecology and Evolution 6(2): 198-208. https://doi.org/10.1111/2041-210X.12301.

Chen, J. M. (1996). Evaluation of vegetation indices and a modified simple ratio for boreal applications. Canadian Journal of Remote Sensing 22(3): 229-242. https://doi.org/10.4095/218303.

Cheng, T., Rivard, B. and Sanchez-Azofeifa, A. (2011). Spectroscopic determination of leaf water content using continuous wavelet analysis. Remote Sensing of Environment 115(2): 659-670. https://doi.org/10.1016/j.rse.2010.11.001.

Cheng, T., Rivard, B., Sánchez-Azofeifa, G., Feng, J. and Calvo-Polanco, M. (2010). Continuous wavelet analysis for the detection of green attack damage due to mountain pine beetle infestation. Remote Sensing of Environment 114(4): 899-910. https://doi.org/10.1016/j.rse.2009.12.005.

Chevone, B. and Linzon, S. (1988). Tree decline in North America. Environmental Pollution 50(1-2): 87-99. https://doi.org/10.1016/0269-7491(88)90186-8.

Choat, B., Jansen, S., Brodribb, T. J., Cochard, H., Delzon, S., Bhaskar, R., Bucci, S. J., Feild, T. S., Gleason, S. M. and Hacke, U. G. (2012). Global convergence in the vulnerability of forests to drought. Nature 491(7426): 752. https://doi.org/10.1038/nature11688.

Chuvieco, E., Cocero, D., Riano, D., Martin, P., Martınez-Vega, J., de la Riva, J. and Perez, F. (2004). Combining NDVI and surface temperature for the estimation of live fuel moisture content in forest fire danger rating. Remote Sensing of Environment 92(3): 322-331. https://doi.org/10.1016/j.rse.2004.01.019.

Chuvieco, E., Riano, D., Aguado, I. and Cocero, D. (2002). Estimation of fuel moisture content from multitemporal analysis of Landsat Thematic Mapper reflectance data: applications in fire danger assessment. International Journal of Remote Sensing 23(11): 2145-2162. https://doi.org/10.1080/01431160110069818.

Coops, N. C., Johnson, M., Wulder, M. A. and White, J. C. (2006). Assessment of QuickBird high spatial resolution imagery to detect red attack damage due to mountain pine beetle infestation. Remote Sensing of Environment 103(1): 67-80. https://doi.org/10.1016/j.rse.2006.03.012.

Danson, F., Steven, M., Malthus, T. and Clark, J. (1992). High-spectral resolution data for determining leaf water content. International Journal of Remote Sensing 13(3): 461-470. https://doi.org/10.1080/01431169208904049.

Danson, F. M., Gaulton, R., Armitage, R. P., Disney, M., Gunawan, O., Lewis, P., Pearson, G. and Ramirez, A. F. (2014). Developing a dual-wavelength full-waveform terrestrial laser scanner to characterize forest canopy structure. Agricultural and Forest Meteorology 198: 7-14. https://doi.org/10.1016/j.agrformet.2014.07.007.

Danson, F. M., Hetherington, D., Morsdorf, F., Koetz, B. and Allgower, B. (2007). Forest canopy gap fraction from terrestrial laser scanning. IEEE Geoscience and Remote Sensing Letters 4(1): 157-160. https://doi.org/10.1109/LGRS.2006.887064.

Datt, B. (1999). Remote sensing of water content in Eucalyptus leaves. Australian Journal of Botany 47(6): 909-923. https://doi.org/10.1071/BT98042.

Dittmar, C., Zech, W. and Elling, W. (2003). Growth variations of common beech (*Fagus sylvatica* L.) under different climatic and environmental conditions in Europe—a

dendroecological study. Forest Ecology and Management 173(1-3): 63-78. https://doi.org/10.1016/S0378-1127(01)00816-7.

Du, L., Gong, W., Shi, S., Yang, J., Sun, J., Zhu, B. and Song, S. (2016). Estimation of rice leaf nitrogen contents based on hyperspectral LIDAR. International Journal of Applied Earth Observation and Geoinformation 44: 136-143. https://doi.org/10.1016/j.jag.2015.08.008.

Easlon, H. M. and Bloom, A. J. (2014). Easy Leaf Area: Automated digital image analysis for rapid and accurate measurement of leaf area. Applications in plant sciences 2(7). https://doi.org/10.3732/apps.1400033.

Eitel, J. U., Höfle, B., Vierling, L. A., Abellán, A., Asner, G. P., Deems, J. S., Glennie, C. L., Joerg, P. C., LeWinter, A. L. and Magney, T. S. (2016). Beyond 3-D: The new spectrum of lidar applications for earth and ecological sciences. Remote Sensing of Environment 186: 372-392. https://doi.org/10.1016/j.rse.2016.08.018.

Eitel, J. U., Magney, T. S., Vierling, L. A., Brown, T. T. and Huggins, D. R. (2014). LiDAR based biomass and crop nitrogen estimates for rapid, non-destructive assessment of wheat nitrogen status. Field Crops Research 159: 21-32. https://doi.org/10.1016/j.fcr.2014.01.008.

Eitel, J. U., Vierling, L. A. and Long, D. S. (2010). Simultaneous measurements of plant structure and chlorophyll content in broadleaf saplings with a terrestrial laser scanner. Remote Sensing of Environment 114(10): 2229-2237. https://doi.org/10.1016/j.rse.2010.04.025.

Ellison, D., Morris, C. E., Locatelli, B., Sheil, D., Cohen, J., Murdiyarso, D., Gutierrez, V., Van Noordwijk, M., Creed, I. F. and Pokorny, J. (2017). Trees, forests and water: Cool insights for a hot world. Global Environmental Change 43: 51-61. https://doi.org/10.1016/j.gloenvcha.2017.01.002.

Elsherif, A., Gaulton, R. and Mills, J. (2018). Estimation of vegetation water content at leaf and canopy level using dual-wavelength commercial terrestrial laser scanners. Interface focus 8(2): 20170041. https://doi.org/10.1098/rsfs.2017.0041.

FAO. (2018). The State of the World's Forests 2018 - Forest pathways to sustainable development, Rome.

Fassnacht, F. E., Latifi, H., Ghosh, A., Joshi, P. K. and Koch, B. (2014). Assessing the potential of hyperspectral imagery to map bark beetle-induced tree mortality. Remote Sensing of Environment 140: 533-548. https://doi.org/10.1016/j.rse.2013.09.014.

Feret, J.-B., François, C., Asner, G. P., Gitelson, A. A., Martin, R. E., Bidel, L. P., Ustin, S. L., le Maire, G. and Jacquemoud, S. (2008). PROSPECT-4 and 5: Advances in the leaf optical properties model separating photosynthetic pigments. Remote Sensing of Environment 112(6): 3030-3043. https://doi.org/10.1016/j.rse.2008.02.012.

Flener, C., Vaaja, M., Jaakkola, A., Krooks, A., Kaartinen, H., Kukko, A., Kasvi, E., Hyyppä, H., Hyyppä, J. and Alho, P. (2013). Seamless mapping of river channels at

high resolution using mobile LiDAR and UAV-photography. Remote Sensing 5(12): 6382-6407. https://doi.org/10.3390/rs5126382.

Foster, A. C., Walter, J. A., Shugart, H. H., Sibold, J. and Negron, J. (2017). Spectral evidence of early-stage spruce beetle infestation in Engelmann spruce. Forest Ecology and Management 384: 347-357. https://doi.org/10.1016/j.foreco.2016.11.004.

Fritts, H. (1976). Tree rings and climate. San Diego, California, Academic. 567 p.

Gaulton, R., Danson, F., Ramirez, F. and Gunawan, O. (2013). The potential of dual-wavelength laser scanning for estimating vegetation moisture content. Remote Sensing of Environment 132: 32-39. https://doi.org/10.1016/j.rse.2013.01.001.

Giannetti, F., Chirici, G., Gobakken, T., Næsset, E., Travaglini, D. and Puliti, S. (2018). A new approach with DTM-independent metrics for forest growing stock prediction using UAV photogrammetric data. Remote Sensing of Environment 213: 195-205. https://doi.org/10.1016/j.rse.2018.05.016.

Gillies, R., Kustas, W. and Humes, K. (1997). A verification of the'triangle'method for obtaining surface soil water content and energy fluxes from remote measurements of the Normalized Difference Vegetation Index (NDVI) and surface. International Journal of Remote Sensing 18(15): 3145-3166. https://doi.org/10.1080/014311697217026.

Hakala, T., Suomalainen, J., Kaasalainen, S. and Chen, Y. (2012). Full waveform hyperspectral LiDAR for terrestrial laser scanning. Optics Express 20(7): 7119-7127. https://doi.org/10.1364/OE.20.007119.

Hanewinkel, M., Cullmann, D. A., Schelhaas, M.-J., Nabuurs, G.-J. and Zimmermann, N. E. (2013). Climate change may cause severe loss in the economic value of European forest land. Nature climate change 3(3): 203-207. https://doi.org/10.1038/nclimate1687.

Hesketh, J. D. (1963). Hesketh JD & Moss D N. Variation in the response of photosynthesis to light. Crop Sci. 3: 107-10, 1963. Crop Science 3: 107-110. https://doi.org/10.2135/cropsci1963.0011183X000300020002x.

Horntvedt, R., Christiansen, E., Solheim, H. and Wang, S. (1983). Artificial inoculation with *Ips typographus*-associated blue-stain fungi can kill healthy Norway spruce trees. 38(4): 1-20.

Houghton, R. A. and Nassikas, A. A. (2018). Negative emissions from stopping deforestation and forest degradation, globally. Global Change Biology 24(1): 350-359. https://doi.org/10.1111/gcb.13876.

Hovi, A. (2015). Towards an enhanced understanding of airborne LiDAR measurements of forest vegetation, Dissertationes Forestales 200. 69 p. https://doi.org/10.14214/df.200.

Huo, L. and Zhang, X. (2019). A new method of equiangular sectorial voxelization of single-scan terrestrial laser scanning data and its applications in forest defoliation estimation. ISPRS Journal of Photogrammetry and Remote Sensing 151: 302-312. https://doi.org/10.1016/j.isprsjprs.2019.03.018.

Hyyppä, J., Hyyppä, H., Leckie, D., Gougeon, F., Yu, X. and Maltamo, M. (2008). Review of methods of small-footprint airborne laser scanning for extracting forest inventory data in boreal forests. International Journal of Remote Sensing 29(5): 1339-1366. https://doi.org/10.1080/01431160701736489.

Immitzer, M. and Atzberger, C. (2014). Early detection of bark beetle infestation in Norway spruce (*Picea abies*, L.) using worldView-2 data frühzeitige erkennung von borkenkä ferbefall an fichten mittels worldView-2 satellitendaten. Photogrammetrie-Fernerkundung-Geoinformation 2014(5): 351-367. https://doi.org/10.1127/1432-8364/2014/0229.

Jacquemoud, S. and Baret, F. (1990). PROSPECT: A model of leaf optical properties spectra. Remote Sensing of Environment 34(2): 75-91. https://doi.org/10.1016/0034-4257(90)90100-Z.

Jactel, H., Petit, J., Desprez-Loustau, M. L., Delzon, S., Piou, D., Battisti, A. and Koricheva, J. (2012). Drought effects on damage by forest insects and pathogens: a meta-analysis. Global Change Biology 18(1): 267-276. https://doi.org/10.1111/j.1365-2486.2011.02512.x.

Jurskis, V. (2005). Eucalypt decline in Australia, and a general concept of tree decline and dieback. Forest Ecology and Management 215(1-3): 1-20. https://doi.org/10.1016/j.foreco.2005.04.026.

Kaasalainen, S., Ahokas, E., Hyyppä, J. and Suomalainen, J. (2005). Study of surface brightness from backscattered laser intensity: calibration of laser data. IEEE Geoscience and Remote Sensing Letters 2(3): 255-259. https://doi.org/10.1109/LGRS.2005.850534.

Kaasalainen, S., Hyyppä, H., Kukko, A., Litkey, P., Ahokas, E., Hyyppä, J., Lehner, H., Jaakkola, A., Suomalainen, J. and Akujärvi, A. (2009). Radiometric calibration of LIDAR intensity with commercially available reference targets. IEEE Transactions on Geoscience and Remote Sensing 47(2): 588-598. https://doi.org/10.1109/TGRS.2008.2003351.

Kaasalainen, S., Jaakkola, A., Kaasalainen, M., Krooks, A. and Kukko, A. (2011). Analysis of incidence angle and distance effects on terrestrial laser scanner intensity: Search for correction methods. Remote Sensing 3(10): 2207-2221. https://doi.org/10.3390/rs3102207.

Kaasalainen, S., Kukko, A., Lindroos, T., Litkey, P., Kaartinen, H., Hyyppa, J. and Ahokas, E. (2008). Brightness measurements and calibration with airborne and terrestrial laser scanners. IEEE Transactions on Geoscience and Remote Sensing 46(2): 528-534. https://doi.org/10.1109/TGRS.2007.911366.

Kaasalainen, S., Nevalainen, O., Hakala, T. and Anttila, K. (2016). Incidence Angle Dependency of Leaf Vegetation Indices from Hyperspectral Lidar Measurements. Photogrammetrie-Fernerkundung-Geoinformation 2016(2): 75-84. https://doi.org/10.1127/pfg/2016/0287.

Kaasalainen, S., Niittymaki, H., Krooks, A., Koch, K., Kaartinen, H., Vain, A. and Hyyppa, H. (2010). Effect of target moisture on laser scanner intensity. IEEE Transactions on Geoscience and Remote Sensing 48(4): 2128-2136. https://doi.org/10.1109/TGRS.2009.2036841.

Kaasalainen, S., Åkerblom, M., Nevalainen, O., Hakala, T. and Kaasalainen, M. (2018). Uncertainty in multispectral lidar signals caused by incidence angle effects. Interface focus 8(2): 20170033. https://doi.org/10.1098/rsfs.2017.0033.

Kandler, O. (1992). The German forest decline situation: a complex disease or a complex of diseases. Forest decline concepts. APS, St Paul, Minn.

Kantola, T., Vastaranta, M., Lyytikäinen-Saarenmaa, P., Holopainen, M., Kankare, V., Talvitie, M. and Hyyppä, J. (2013). Classification of needle loss of individual Scots pine trees by means of airborne laser scanning. Forests 4(2): 386-403. https://doi.org/10.3390/f4020386.

Kashani, A. G., Olsen, M. J., Parrish, C. E. and Wilson, N. (2015). A review of LiDAR radiometric processing: From ad hoc intensity correction to rigorous radiometric calibration. Sensors 15(11): 28099-28128. https://doi.org/10.3390/s151128099.

Kennedy, R. E., Yang, Z. and Cohen, W. B. (2010). Detecting trends in forest disturbance and recovery using yearly Landsat time series: 1. LandTrendr—Temporal segmentation algorithms. Remote Sensing of Environment 114(12): 2897-2910. https://doi.org/10.1016/j.rse.2010.07.008.

Kohler, M., Sohn, J., Nägele, G. and Bauhus, J. (2010). Can drought tolerance of Norway spruce (*Picea abies* (L.) Karst.) be increased through thinning? European Journal of Forest Research 129(6): 1109-1118. https://doi.org/10.1007/s10342-010-0397-9.

Korpela, I. (2017). Acquisition and evaluation of radiometrically comparable multi-footprint airborne LiDAR data for forest remote sensing. Remote Sensing of Environment 194: 414-423. https://doi.org/10.1016/j.rse.2016.10.052.

Kreutzer, K. (1993). Changes in the role of nitrogen in Central European forests. In: Forest decline in the Atlantic and Pacific Region. Springer, Berlin p. 82-96. https://doi.org/10.1007/978-3-642-76995-5_6.

Krooks, A., Kaasalainen, S., Hakala, T. and Nevalainen, O. (2013). Correction of intensity incidence angle effect in terrestrial laser scanning. ISPRS Annals of the Photogrammetry, Remote Sensing and Spatial Information Sciences 2: 145-150. https://doi.org/10.5194/isprsannals-II-5-W2-145-2013.

Kukko, A., Kaartinen, H., Hyyppä, J. and Chen, Y. (2012). Multiplatform mobile laser scanning: Usability and performance. Sensors 12(9): 11712-11733. https://doi.org/10.3390/s120911712.

Lausch, A., Erasmi, S., King, D. J., Magdon, P. and Heurich, M. (2017). Understanding forest health with remote sensing-part II—a review of approaches and data models. Remote Sensing 9(2): 129. https://doi.org/10.3390/rs9020129.

Lausch, A., Heurich, M., Gordalla, D., Dobner, H.-J., Gwillym-Margianto, S. and Salbach, C. (2013). Forecasting potential bark beetle outbreaks based on spruce forest vitality using hyperspectral remote-sensing techniques at different scales. Forest Ecology and Management 308: 76-89. https://doi.org/10.1016/j.foreco.2013.07.043.

LeBlanc, D. C., Nicholas, N. and Zedaker, S. (1992). Prevalence of individual-tree growth decline in red spruce populations of the southern Appalachian Mountains. Canadian Journal of Forest Research 22(6): 905-914. https://doi.org/10.1139/x92-120.

Lemmens, M. (2011). Terrestrial laser scanning. In: Geo-information. Springer, Dordrecht p. 101-121. https://doi.org/10.1007/978-94-007-1667-4_6.

Liang, X., Hyyppä, J., Kaartinen, H., Lehtomäki, M., Pyörälä, J., Pfeifer, N., Holopainen, M., Brolly, G., Francesco, P. and Hackenberg, J. (2018). International benchmarking of terrestrial laser scanning approaches for forest inventories. ISPRS Journal of Photogrammetry and Remote Sensing 144: 137-179. https://doi.org/10.1016/j.isprsjprs.2018.06.021.

Lin, Y., Hyyppa, J. and Jaakkola, A. (2011). Mini-UAV-borne LIDAR for fine-scale mapping. IEEE Geoscience and Remote Sensing Letters 8(3): 426-430. https://doi.org/10.1109/LGRS.2010.2079913.

Magney, T. S., Eusden, S. A., Eitel, J. U., Logan, B. A., Jiang, J. and Vierling, L. A. (2014). Assessing leaf photoprotective mechanisms using terrestrial LiDAR: towards mapping canopy photosynthetic performance in three dimensions. New Phytologist 201(1): 344-356. https://doi.org/10.1111/nph.12453.

McCutchan, H. and Shackel, K. (1992). Stem-water potential as a sensitive indicator of water stress in prune trees (*Prunus domestica* L. cv. French). Journal of the American Society for Horticultural Science 117(4): 607-611. https://doi.org/10.21273/JASHS.117.4.607.

Naesset, E. (1997). Estimating timber volume of forest stands using airborne laser scanner data. Remote Sensing of Environment 61(2): 246-253. https://doi.org/10.1016/S0034-4257(97)00041-2.

Näsi, R., Honkavaara, E., Blomqvist, M., Lyytikäinen-Saarenmaa, P., Hakala, T., Viljanen, N., Kantola, T. and Holopainen, M. (2018). Remote sensing of bark beetle damage in urban forests at individual tree level using a novel hyperspectral camera from UAV and aircraft. Urban Forestry & Urban Greening 30: 72-83. https://doi.org/10.1016/j.ufug.2018.01.010.

Näsi, R., Honkavaara, E., Lyytikäinen-Saarenmaa, P., Blomqvist, M., Litkey, P., Hakala, T., Viljanen, N., Kantola, T., Tanhuanpää, T. and Holopainen, M. (2015). Using UAV-Based Photogrammetry and Hyperspectral Imaging for Mapping Bark Beetle Damage at Tree-Level. Remote Sensing 7(11): 15467-15493. https://doi.org/10.3390/rs71115467.

Netherer, S. and Schopf, A. (2010). Potential effects of climate change on insect herbivores in European forests—general aspects and the pine processionary moth as specific

example. Forest Ecology and Management 259(4): 831-838. https://doi.org/10.1016/j.foreco.2009.07.034.

Nevalainen, O., Hakala, T., Suomalainen, J. and Kaasalainen, S. (2013). Nitrogen concentration estimation with hyperspectral LiDAR. ISPRS Annals of the Photogrammetry, Remote Sensing and Spatial Information Sciences, II-5 W 2: 205-210. https://doi.org/10.5194/isprsannals-II-5-W2-205-2013.

Nevalainen, O., Hakala, T., Suomalainen, J., Mäkipää, R., Peltoniemi, M., Krooks, A. and Kaasalainen, S. (2014). Fast and nondestructive method for leaf level chlorophyll estimation using hyperspectral LiDAR. Agricultural and Forest Meteorology 198: 250-258. https://doi.org/10.1016/j.agrformet.2014.08.018.

Niemann, K. O., Quinn, G., Stephen, R., Visintini, F. and Parton, D. (2015). Hyperspectral remote sensing of mountain pine beetle with an emphasis on previsual assessment. Canadian Journal of Remote Sensing 41(3): 191-202. https://doi.org/10.1080/07038992.2015.1065707.

O'Reilly-Wapstra, J. M., McArthur, C., Potts, B., Iason, G., Dicke, M. and Hartley, S. (2012). Natural selection for anti-herbivore plant secondary metabolites: a Eucalyptus system. In: The ecology of plant secondary metabolites: genes to global processes. Cambridge University Press, London p. 10-33. https://doi.org/10.1017/CBO9780511675751.003.

Peñuelas, J., Pinol, J., Ogaya, R. and Filella, I. (1997). Estimation of plant water concentration by the reflectance water index WI (R900/R970). International Journal of Remote Sensing 18(13): 2869-2875. https://doi.org/10.1080/014311697217396.

Poorter, H., Niinemets, Ü., Poorter, L., Wright, I. J. and Villar, R. (2009). Causes and consequences of variation in leaf mass per area (LMA): a meta-analysis. New Phytologist 182(3): 565-588. https://doi.org/10.1111/j.1469-8137.2009.02830.x.

Poullain, E., Garestier, F., Levoy, F. and Bretel, P. (2016). Analysis of ALS Intensity Behavior as a Function of the Incidence Angle in Coastal Environments. IEEE Journal of Selected Topics in Applied Earth Observations and Remote Sensing 9(1): 313-325. https://doi.org/10.1109/JSTARS.2015.2510337.

Qi, W. and Dubayah, R. O. (2016). Combining Tandem-X InSAR and simulated GEDI lidar observations for forest structure mapping. Remote Sensing of Environment 187: 253-266. https://doi.org/10.1016/j.rse.2016.10.018.

R Core Team. (2013). A language and environment for statistical computing. R Foundation for Statistical Computing, Vienna, Austria.

Radeloff, V. C., Mladenoff, D. J. and Boyce, M. S. (1999). Detecting jack pine budworm defoliation using spectral mixture analysis: separating effects from determinants. Remote Sensing of Environment 69(2): 156-169. https://doi.org/10.1016/S0034-4257(99)00008-5.

Ramirez, F. J. R., Navarro-Cerrillo, R. M., Varo-Martínez, M. Á., Quero, J. L., Doerr, S. and Hernández-Clemente, R. (2018). Determination of forest fuels characteristics in mortality-affected *Pinus* forests using integrated hyperspectral and ALS data. International Journal of Applied Earth Observation and Geoinformation 68: 157-167. https://doi.org/10.1016/j.jag.2018.01.003.

Reich, P., Walters, M., Tjoelker, M., Vanderklein, D. and Buschena, C. (1998). Photosynthesis and respiration rates depend on leaf and root morphology and nitrogen concentration in nine boreal tree species differing in relative growth rate. Functional Ecology 12(3): 395-405. https://doi.org/10.1046/j.1365-2435.1998.00209.x.

Schlyter, P., Stjernquist, I., Bärring, L., Jönsson, A. M. and Nilsson, C. (2006). Assessment of the impacts of climate change and weather extremes on boreal forests in northern Europe, focusing on Norway spruce. Climate Research 31(1): 75-84. https://doi.org/10.3354/cr031075.

Schultz, J. C. and Baldwin, I. T. (1982). Oak leaf quality declines in response to defoliation by gypsy moth larvae. Science 217(4555): 149-151. https://doi.org/10.1126/science.217.4555.149.

Schulze, E.-D. (1989). Air pollution and forest decline in a spruce (*Picea abies*) forest. Science 244(4906): 776-783. https://doi.org/10.1007/978-3-642-61332-6.

Schwarz, G. (1978). Estimating the dimension of a model. The annals of statistics 6(2): 461-464. https://doi.org/10.1214/aos/1176344136.

Senf, C., Pflugmacher, D., Wulder, M. A. and Hostert, P. (2015). Characterizing spectral–temporal patterns of defoliator and bark beetle disturbances using Landsat time series. Remote Sensing of Environment 170: 166-177. https://doi.org/10.1016/j.rse.2015.09.019.

Siddique, M., Hamid, A. and Islam, M. (2000). Drought stress effects on water relations of wheat. Botanical Bulletin of Academia Sinica 41.

Sinclair, T. and Ludlow, M. (1985). Who taught plants thermodynamics? The unfulfilled potential of plant water potential. Functional Plant Biology 12(3): 213-217. https://doi.org/10.1071/PP9850213.

Skakun, R. S., Wulder, M. A. and Franklin, S. E. (2003). Sensitivity of the thematic mapper enhanced wetness difference index to detect mountain pine beetle red-attack damage. Remote Sensing of Environment 86(4): 433-443. https://doi.org/10.1016/S0034-4257(03)00112-3.

Sun, J., Shi, S., Gong, W., Yang, J., Du, L., Song, S., Chen, B. and Zhang, Z. (2017). Evaluation of hyperspectral LiDAR for monitoring rice leaf nitrogen by comparison with multispectral LiDAR and passive spectrometer. Scientific Reports 7: 40362. https://doi.org/10.1038/srep40362.

Sun, J., Shi, S., Yang, J., Chen, B., Gong, W., Du, L., Mao, F. and Song, S. (2018). Estimating leaf chlorophyll status using hyperspectral lidar measurements by

PROSPECT model inversion. Remote Sensing of Environment 212: 1-7. https://doi.org/10.1016/j.rse.2018.04.024.

Tan, K. and Cheng, X. (2016). Correction of incidence angle and distance effects on TLS intensity data based on reference targets. Remote Sensing 8(3): 251. https://doi.org/10.3390/rs8030251.

Toth, C. K. and Petrie, G. (2018). Terrestrial laser scanners. In: Topographic Laser Ranging and Scanning. CRC Press, p. 29-88. https://doi.org/10.1201/9781315154381-2.

Trumbore, S., Brando, P. and Hartmann, H. (2015). Forest health and global change. Science 349(6250): 814-818. https://doi.org/10.1126/science.aac6759.

Tucker, C. J. (1980). Remote sensing of leaf water content in the near infrared. Remote Sensing of Environment 10(1): 23-32. https://doi.org/10.1016/0034-4257(80)90096-6.

Wagner, W., Ullrich, A., Ducic, V., Melzer, T. and Studnicka, N. (2006). Gaussian decomposition and calibration of a novel small-footprint full-waveform digitising airborne laser scanner. ISPRS Journal of Photogrammetry and Remote Sensing 60(2): 100-112. https://doi.org/10.1016/j.isprsjprs.2005.12.001.

Van Gelder, H., Poorter, L. and Sterck, F. (2006). Wood mechanics, allometry, and life-history variation in a tropical rain forest tree community. New Phytologist 171(2): 367-378. https://doi.org/10.1111/j.1469-8137.2006.01757.x.

Wang, J., Sammis, T. W., Gutschick, V. P., Gebremichael, M., Dennis, S. O. and Harrison, R. E. (2010). Review of satellite remote sensing use in forest health studies. The Open Geography Journal 3(1). https://doi.org/10.2174/1874923201003010028.

Waring, R. and Pitman, G. (1985). Modifying lodgepole pine stands to change susceptibility to mountain pine beetle attack. Ecology 66(3): 889-897. https://doi.org/10.2307/1940551.

Waring, R. H. (1983). Estimating forest growth and efficiency in relation to canopy leaf area. In: Advances in Ecological Research. Elsevier. 13 p. 327-354. https://doi.org/10.1016/S0065-2504(08)60111-7.

Watson, D. (1958). The dependence of net assimilation rate on leaf-area index. Annals of Botany 22(1): 37-54. https://doi.org/10.1093/oxfordjournals.aob.a083596.

Wermelinger, B. (2004). Ecology and management of the spruce bark beetle *Ips typographus* — a review of recent research. Forest Ecology and Management 202(1): 67-82. https://doi.org/10.1016/j.foreco.2004.07.018.

Williams, A. P., Allen, C. D., Macalady, A. K., Griffin, D., Woodhouse, C. A., Meko, D. M., Swetnam, T. W., Rauscher, S. A., Seager, R. and Grissino-Mayer, H. D. (2013). Temperature as a potent driver of regional forest drought stress and tree mortality. Nature climate change 3(3): 292-297. https://doi.org/10.1038/nclimate1693.

Vogelmann, J. E., Xian, G., Homer, C. and Tolk, B. (2012). Monitoring gradual ecosystem change using Landsat time series analyses: Case studies in selected forest and rangeland ecosystems. Remote Sensing of Environment 122: 92-105. https://doi.org/10.1016/j.rse.2011.06.027.

Wulder, M. A., Dymond, C. C., White, J. C., Leckie, D. G. and Carroll, A. L. (2006). Surveying mountain pine beetle damage of forests: A review of remote sensing opportunities. Forest Ecology and Management 221(1): 27-41. https://doi.org/10.1016/j.foreco.2005.09.021.

Yu, X., Hyyppä, J., Litkey, P., Kaartinen, H., Vastaranta, M. and Holopainen, M. (2017). Single-Sensor Solution to Tree Species Classification Using Multispectral Airborne Laser Scanning. Remote Sensing 9(2): 108. https://doi.org/10.3390/rs9020108.

Zhu, X., Wang, T., Darvishzadeh, R., Skidmore, A. K. and Niemann, K. O. (2015). 3D leaf water content mapping using terrestrial laser scanner backscatter intensity with radiometric correction. ISPRS Journal of Photogrammetry and Remote Sensing 110: 14-23. https://doi.org/10.1016/j.isprsjprs.2015.10.001.

Zhu, X., Wang, T., Skidmore, A. K., Darvishzadeh, R., Niemann, K. O. and Liu, J. (2017). Canopy leaf water content estimated using terrestrial LiDAR. Agricultural and Forest Meteorology 232: 152-162. https://doi.org/10.1016/j.agrformet.2016.08.016.

122 references